

POLITECNICO DI TORINO

Energy Department

**Master Degree in Energy and Nuclear
Engineering**

Master's Degree Thesis

**Water extraction from atmospheric air:
CFD model of an adsorption heat exchanger**



Supervisors

Prof. Marco Simonetti

Prof. Giovanni Vincenzo Fracastoro

Ing. Vincenzo Gentile

Student

Luca Agnoletti

A.Y. 2017/2018

Contents

Contents	1
1 Introduction	5
1.1 Water demand	7
1.2 Desalination	9
1.2.1 State of Art	10
1.2.2 Energy and environmental impacts of desalination plants	16
1.3 Water harvesting from atmosphere	18
2 Water Harvesting Cycle	21
2.1 Thermodynamic cycle	21
2.2 Prototype configuration	24
2.3 Adsorption Heat Exchanger	26
2.4 Adsorption materials	28
2.5 Geometry optimization	35
3 Introduction to CFD	37
3.1 CFD code structure	38
3.1.1 Pre-processor	38
3.1.2 Solver	39
3.1.3 Post-processor	40
3.2 Fluid dynamics equations	41
3.2.1 Conservation of the mass	41
3.2.2 Momentum equations	43

3.2.3	Energy equations	44
4	Adsorption model with STAR-CCM+	47
4.1	Model description	48
4.1.1	Experimental determination of Silica gel Isotherms	51
4.2	Silica gel simulation	56
4.2.1	Comparison with experimental test	66
4.2.2	Simulation with the temperature of the spheres	73
5	Extension of the model for a coated HX-ADS	79
5.1	Simulation of an adsorbent coating in a finned heat exchanger	81
6	Conclusions	91
	Bibliography	95

Nomenclature

CFD	[-]	Computational fluid dynamics
cp_{sil}	[$kJ/kg/K$]	Specific heat at constant pressure of the silica gel
D	[mm]	Distance between two successive fins
D_H	[m]	Hydraulic diameter
D_{H_2O}	[m^2/s]	Apparent diffusion of the vapour inside the silica gel pores
DEC	[-]	Desiccant evaporative cooling
E	[-]	Energy
ED	[-]	Electrodialysis
EDR	[-]	Electrodialysis Reversal
FO	[-]	Forward Osmosis
GOR	[-]	Gained Output Ratio
H	[kJ/kg]	Heat of vaporization
HDH	[-]	Humidification Dehumidification
HX-ADS	[-]	Adsorption heat exchanger
k	[$W/m/K$]	Thermal conductivity
\dot{m}_{H_2O}	[$kg/m^2/s$]	Mass flux on the adsorbent surface
MED	[-]	Multi-effect Distillation
MOFs	[-]	Metal-organic frameworks
MSF	[-]	Multistage Flash
NF	[-]	Nanofiltration
p	[Pa]	Pressure
p_a	[Pa]	Ambient pressure
$p_{v_{sat}}$	[Pa]	Saturated vapour pressure
p_{eq}	[Pa]	Vapour partial pressure of air mixture in the condition with silica gel moisture content

p_v	[Pa]	Vapour partial pressure of vapour air mixture
PCPs	[-]	Porous coordination polymers
\dot{q}_{ads}	[[W/m ²]]	Adsorption specific heat flux
RH_{eq}	[-]	Air relative humidity in equilibrium condition
RH_{in}	[-]	Air relative humidity at the inlet
RH	[-]	Air relative humidity
RO	[-]	Reverse Osmosis
Re	[-]	Reynolds number
S_M	[-]	Source term in the momentum equation
S_E	[-]	Source term in the energy equation
SWSs	[-]	Selective water sorbents
t	[s]	Time
Δt	[s]	Time step used for the CFD simulation
T_{air-in}	[°C]	Temperature of the air at the inlet
$T_{cold-water}$	[°C]	Temperature of the cold in the recirculating pipes during adsorption
$T_{hot-water}$	[°C]	Temperature of the hot in the recirculating pipes during regeneration
T_s	[°C]	Temperature of the adsorbent
u	[m/s]	Velocity along the x-axis
v	[m/s]	Velocity along the y-axis
v_{in}	[m/s]	Velocity of the air at the inlet
V_c	[m ³]	Volume of adsorbent material related to a single cell
w	[m/s]	Velocity along the z-axis
W	[kg _{water} /kg _{dry} sorbent]	Water uptake
W_0	[kg _{water} /kg _{dry} sorbent]	Initial water uptake
$W^*(T, HR)$	[kg]	Weight of adsorption material at a certain temperature and air relative humidity
W_{dry}^*	[kg]	Weight of adsorption material in dry condition
x	[kg _{vapour} /kg _{air}]	Moisture content of the vapour air mixture
x	[kg _{vapour} /kg _{air}]	Equilibrium air moisture content
μ_{air}	[Pa · s]	Dynamic viscosity of the air
ρ	[kg/m ³]	Density
ρ_{air}	[kg/m ³]	Density of the air
ρ_s	[kg/m ³]	Density of adsorption material
ρ_{sil}	[kg/m ³]	Density of silica gel
τ	[Pa]	Viscous stress

Chapter 1

Introduction

The fulfillment of water demand relies on the consume of natural and renewable resources: rivers, lakes and groundwater. In some regions of the world, the intensive use of these resources affected the natural water cycle, disturbing the natural recovery through the rainfall. The risk of unavailability can affect also countries that normally do not face drought problems.

The global population increase is the main reason of the increase resources demand. For this reason, many studies stress the attention on the problem monitoring all over the world the availability of fresh water in particular for such sectors as industry and agriculture, that are potential obstacle for a direct access to clean and safe water for the population. The scale of the problem is global, all users and industries need to safeguard water supplies throughout the world in order to limit the lack of availability of clean water. The main common goal is to guarantee enough safe and sustainable water for the global human consumption and, in parallel, the industrial utilization must be controlled with safeguarding policies based on the reuse and recycling of the waste water. Indeed industry can reduce the consumption of fresh water, for example reusing more of the wastewater produced as a process's product, and try to use alternative water source [\[1\]](#).

Further on, in some regions, because of the unfavorable climatic condition, the drought is an actual problem. For instance, the California's drought (2011-2016) led to a dramatic drop of the main dammed lakes of Western U.S., the Mead Lake.

Indeed, in July 2016 it reached the lowest water level^{[3][2]}. Another critical situation is the Cape Town water crisis in which scientists estimates that it will be the first major city in the world to run out of water^[4].

These examples highlight that the deeper use of conventional resources cannot be a solution anymore. For these reasons the scientific and technological development has the goal to realize feasible and efficient systems providing water exploiting “alternative resources”:

- Harvested rainwater from roofs
- Onsite stormwater
- Discharged water from industrial processes
- Desalination of sea water
- Extraction of water from air

At the moment, to reach the requirement in potable water supply, we have to consider the desalination systems as the most developed, and used, technology nowadays in order to have an alternative fresh water source. However this type of process presents some drawbacks, as an high consumption of fossil fuel, so other ways to obtain fresh water are studied.

In conclusion, to control the water consumption for the next decades we have to use in a conscious and sustainable way all standard and alternative fresh water resources. In this work, I studied a system of water extraction from atmospheric air, based on adsorption materials. In particular, a prototype of this system was already assembled in the laboratory of the Energy Department of the Polytechnic of Turin. The goal of this analysis is to produce a CFD model of the system that is able to simulate the system in the actual configuration, and use it as a design instrument to explore several layouts and evaluate advantages and disadvantages in different each configurations. In conclusion, this work permits to study several properties of the system, such as the geometry or the material, and then results can be used to develop an improved version of the existing prototype.

1.1 Water demand

The increase of global population, nevertheless the economic development and the urbanization have induced people to have a higher consumption of resources all around the world. Simultaneously, the globalization have permitted that connections, to the origin of their consumed resources, become weaker. In addition, meat-heavy diets are becoming more and more common^{[5] [6]}, increasing a lot the water demand, and the global population is concentrating in mega-cities, causing a strong disequilibrium on the request of resources in those areas^[7].

For example, analyzing the water consumption related to the food production in Europe, especially in cities located in Mediterranean area, the use of water varies between 3200 and 5800 liters per capita per day. These values are strongly higher related to the urban direct water use that is around 150-300 liters per capita per day. Moreover, the high prevalence of meat based diets compared other types, such as pesco-vegetarian, increasing the water footprint of cities, getting worse the management of the water all around the world.

Additionally, another problem linked to the increase of the water demand, that impacts on a larger scale, is the amount of water related to irrigate agriculture that is increasing a lot due to the growing of the world population. At the same time, while countries are developing their economies, also the industrial sector requires more resources.

This problem, for instance, is very obvious in the power sector where energy and water are inextricably linked and their consumptions grow jointly. Firstly, water is used in each process of the fuel production, such as coal mining, oil extraction, coal liquefaction, power generation, and exhaust gas treatment. Then energy is used for the water extraction and consumption, such as water exploitation, water desalination, and waste water treatment. Due to these factors, is expected an increasing water consumption worldwide in the next decades.

In support of this topic, the Tsinghua University has published an analysis on the China's water demand until 2050^[8].

Results, divided by sub sectors, are show in the following Figure. 1.1

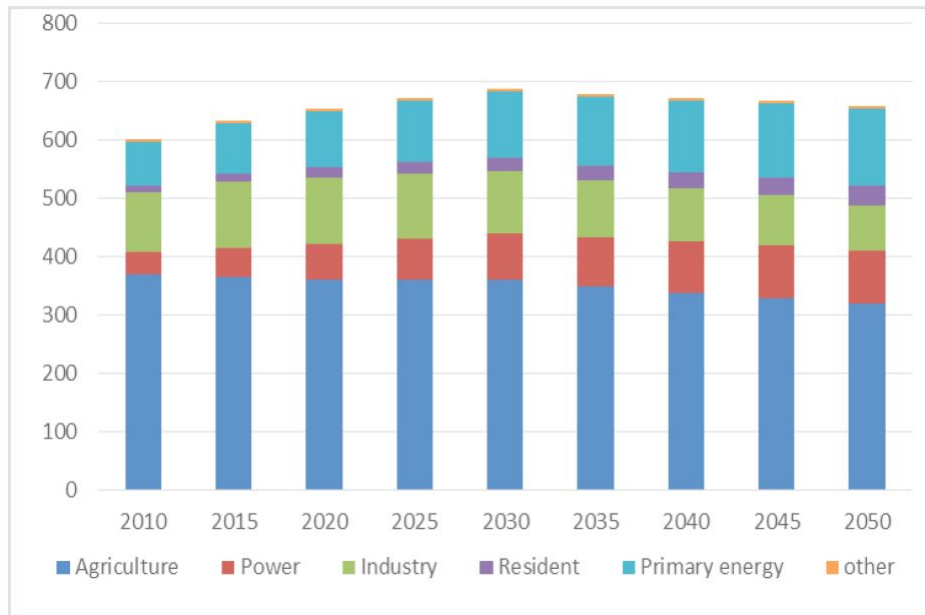


Figure 1.1: The China's water demand by subsectors (billion m^3) [8](#)

Results of the study project a water demand increase from 602 billion m^3 in 2010 to 688 billion m^3 in 2030, and then the requirement changes decreasing until 650 billion m^3 in 2050. In particular this behaviour is related to the total water demand, but for each sector the trend is different in the period under exam.

Starting from the agriculture sector, considering an improvement of irrigation efficiency and a gradually stable food consumption, the water demand will keep decreasing, from 369 billion m^3 in 2010 to 320 billion m^3 in 2050. Related to the total demand, the share will decrease from 62.0% to around 50.0%, but remaining the dominant water user.

A different forecast was obtained for the power sector, in fact with the increasing of the electricity demand, the water demand increasing too during 2010-2050, and the share of water demand will increase from 6.0% to 13.0%.

For the industry sector the trend changes, first increasing and then decreasing, with a peak of 115 billion m^3 around the 2020. This behaviour is related to an improvement of the efficiency of production processes and to different ways to manage the waste water reuse. In the same analysis is show as it can change sup-

posing different water fee in order to facilitate a better water management. For the residential sector the water demand increasing in the whole period due to improvement of living standard and the expanding of urbanization population. Then analyzing the water used in the primary sector, so linked to raw materials, it is observable that the water demand will keep increasing, but the share remains very low [\[8\]](#).

These behaviours underline a common increase for the next twenty years, until 2030-2035, in many sub sectors that implies a total rise in water demand that requires alternative water sources in order to limit the usage of standard water sources.

This problem can be extended to all the developing countries.

This trend involves an increasing of the extraction rate of freshwater from surface water bodies and underground aquifers all over the world, which leads to depletion of the resource, and can possibly cause land subsidence if groundwater is over-extracted. Conventional water resources are no longer sufficient to meet demand.

According to Ng et al . (2013) [\[9\]](#), global water demand is projected to increase at an average annual rate of 2%, leading to a demand of close to 7 trillion m^3 by the year 2030, with a total percentage increase of around 55%, as is illustrated in Figure [1.2](#).

To conclude, the rise of the water demand is an important issue that can cause several problems with dangerous effects on the planet and the global population, so we have to deal with it.

1.2 Desalination

As seen in the previous paragraph there is the need of produce fresh water in an alternative way to reduce its extraction from conventional sources, satisfying anyway the requirement and supplying water also to arid region. As a matter of the fact, part of the world population lives where water availability is not guarantee due to its lack.

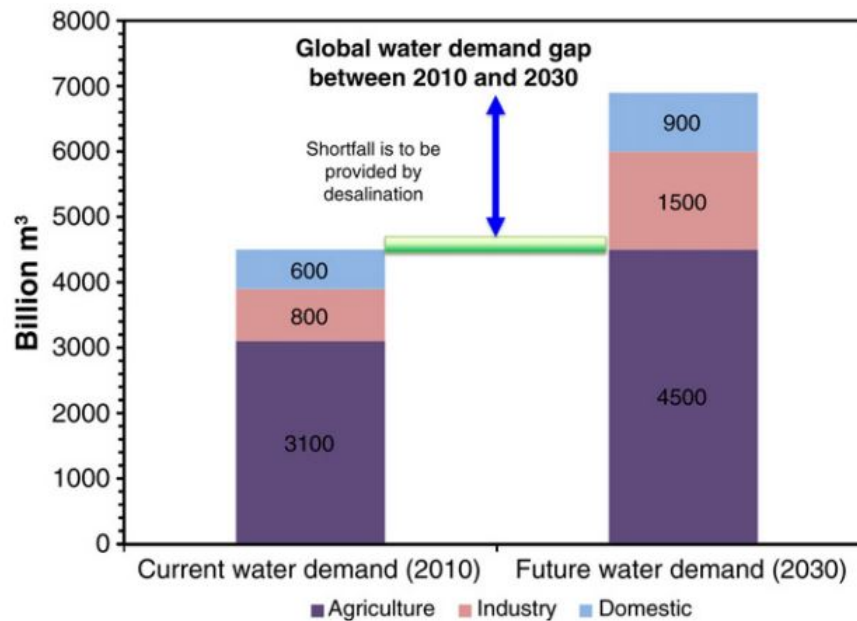


Figure 1.2: The present (2010) and the projected (2030) water demand of the world [\[9\]](#)

Due to this natural fresh water scarcity, desalination has become the major source of fresh water all around the world [\[10\]](#).

1.2.1 State of Art

Desalination processes have the purpose to obtain fresh water starting from salt water. This can be done mainly in two ways defining two categories of desalination systems. On one hand it can be done extracting fresh water while, on the other hand, removing salt from seawater. At the moment the first category prevails on the second one because is the most developed and almost all plants worldwide are based on the extraction of fresh water.

An overview on the desalination methods reported today is shown in table [\[2.1\]](#). In addition, the Figure [\[1.3\]](#) illustrates that, nowadays, the existing plants are based mainly on three of the previous methods. In fact, in 2013, the 65% of the installed

Table 1.1: General desalination methods. [\[13\]](#)

Classification	Methods
Extracting fresh water	<ol style="list-style-type: none"> 1. Distillation <ol style="list-style-type: none"> a. Multi-effect Distillation b. Multistage flash c. Vapor compression distillation d. Solar distillation e. Humidification-dehumidification desalination f. Absorption desalination 2. Freezing(crystallizer based) <ol style="list-style-type: none"> a. Vapor compression freezing b. Vapor absorption freezing c. Direct refrigerant freezing 3. Hydrate desalination (crystallizer based) 4. Solvent extraction desalination 5. Reverse osmosis (membrane based)
Separate salt from seawater	<ol style="list-style-type: none"> 1. Electrodialysis (membrane based) 2. Ion exchanging

systems were Reverse Osmosis plants, while the 22% were Multistage Flash and finally the 8% were Multi-Effect Distillation systems [\[10\]](#).

In brief, these technologies are described below.

Multi-effect Distillation

This method, illustrated in Figure [1.4](#), is based on a series of evaporators, also called "effects". In the first stage the evaporation of the injected seawater takes place thanks to an external heat source, producing the "second steam". Then it is led into the next evaporators for heating again seawater but at a lower temperature. Evaporators operate on the principle of reducing pressure in order not to use intermediate heating from external sources. There is both the production of vapour

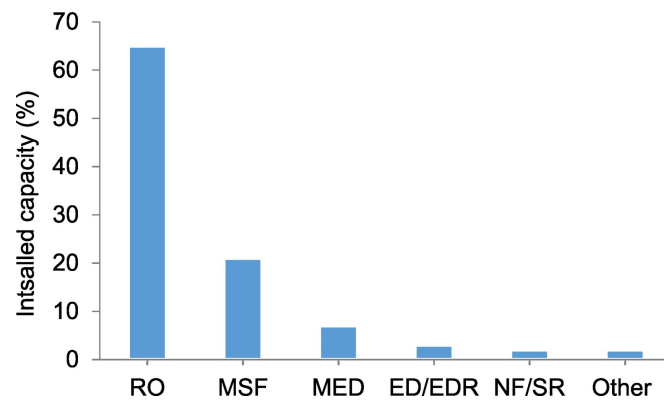


Figure 1.3: Total worldwide installed desalination capacity by technology [\[1\]](#) [\[2\]](#)

and brine for each stage and the produced fresh water is the condensate collected from the second stage. To conclude, this type of technology is characterized by an high efficiency of heat utilization but it requires also high costs of investment [\[3\]](#) [\[4\]](#).

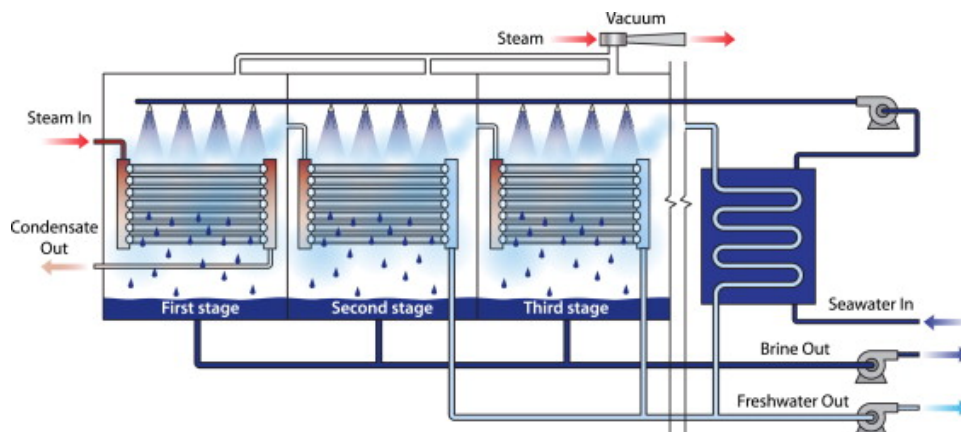


Figure 1.4: Multi-effect Distillation Process [\[4\]](#)

Multistage Flash Distillation

In this process, as shown in Figure [\[1.5\]](#), seawater enters in the system passing through all stages for preheating. After that a final heating is performed with an external heat source and then seawater goes to a low-pressure boiler in which evaporates immediately. Evaporation keeps going in the next stages due to a decreasing pressure. The vapour that is generated in each stage condenses to fresh

water on the external surface of the preheating tube and it is collected as the product of the system.

The advantages of this process are a simple structure and low investment costs but, as drawback, there are high operating costs related to the external heat source and to the periodic cleaning to remove deposits on the tubes.

At the moment this type of technology is the second most desalination process installed all over the world after the RO process [\[13\]](#) [\[14\]](#).

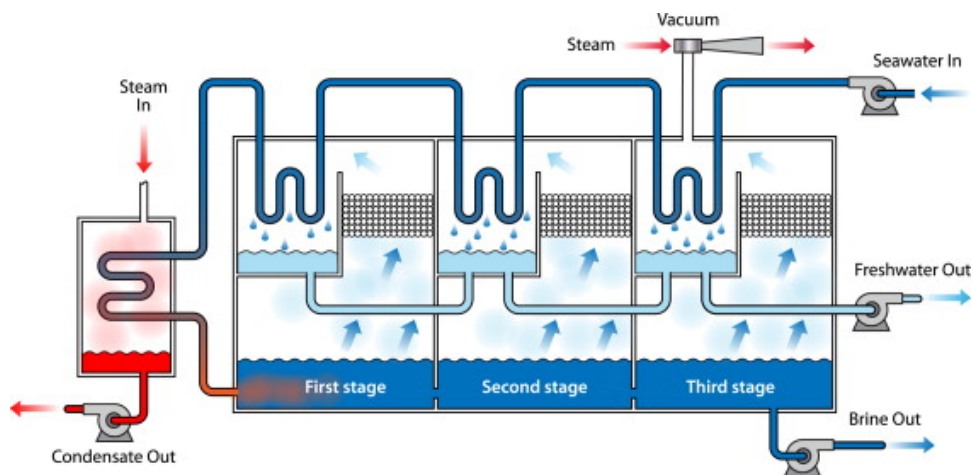


Figure 1.5: Multistage Flash Distillation Process [\[14\]](#)

Reverse Osmosis

In this case the process is different from the other because is not based on distillation, but fresh water is produced only with the usage of a membrane. In addition, this method is noted for no change of phase and it requires only an electrical contribution and not a thermal one.

Seawater is compressed to high pressure, approximately to 25 atm, and it filters in a semi-permeable membrane that allows water to pass through but blocking salt. On the first side of the membrane remains a concentrated solution at high pressure that can be eventually sent to a turbine, as shown in figure [\[1.6\]](#). At the moment, several types of membrane are available on the market and others are studied in order to improve the efficiency of the system requiring a lower contribute

of electrical power and increasing the lifetime of the component.

This technology was subjected to great improvement over the last ten years and other advancement are expected for the next few years [13] [14].

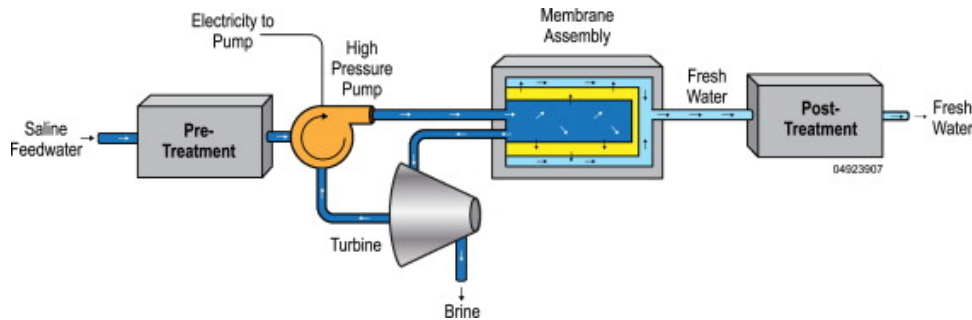


Figure 1.6: Reverse Osmosis Desalination [14]

Other Desalination technologies

The previous three methods cover the majority of the market but also other methods are used. A technique that works well with brackish water is Electrodialysis. It is based on the use of ion-exchange membranes, in particular, alternating anion-exchange and cation-exchange membranes. Then interspaces between two membranes are filled with seawater, as shown in Figure 1.7.

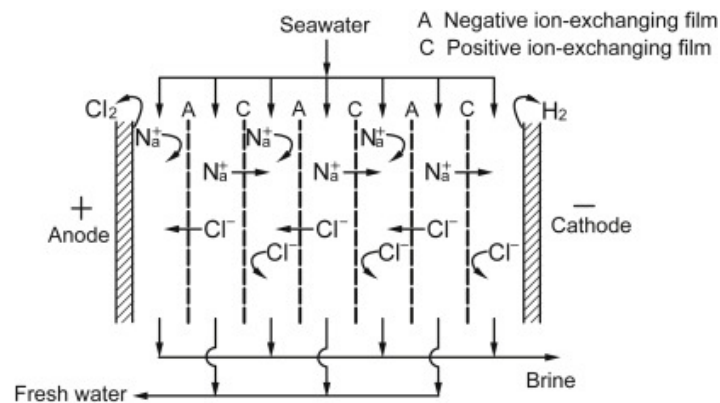


Figure 1.7: Electrodialysis desalination schematic. [13]

Finally, applying an external DC electric field, anions and cations desalinate the seawater in some intervals. This method is advantageous when the salt concen-

tration is below 500 ppm because is more economical respect to other techniques. Problems for large scale applications are that no charge impurities will not be removed and, in addition, the operating costs increase significantly with higher salt concentration. For this reason, at the moment, is not one of the main processes used worldwide.

Other interesting methods for desalination of seawater are Forward Osmosis and Air Humidification and Dehumidification, that can probably become more diffuse in the future but today are playing a minor role in the market due to higher energy consumption compared with commercial technologies.

FO desalination is similar to RO process but the water direction through the membrane is the opposite. In fact water molecules, of the seawater, cross the semipermeable membrane going to the draw solution, which is at higher salt concentration. An example of draw solution is $\text{NH}_3\text{-CO}_2$, as illustrate in Figure 1.8.

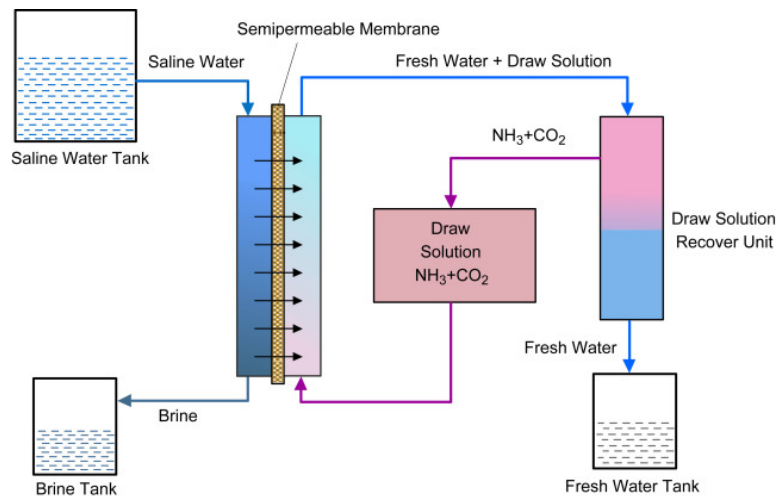


Figure 1.8: Forward osmosis unit using $\text{NH}_3\text{-CO}_2$ as draw solution. ^[13]

In addition membranes used in RO desalination processes are not suitable for FO applications so other studies are requested for this technology ^[13].

To conclude, an interesting solution for the future can be Air Humidification and Dehumidification Desalination (HDH). In this method seawater, after an external preheating, is injected in the system from the top of the humidifier where transfer heat and mass (water) to the carrier gas, typically air. Then the hot and humid

air goes to the dehumidifier in which water condense, exchanging heat with the entering cold seawater.

A scheme of this process is illustrate in Figure 1.9.

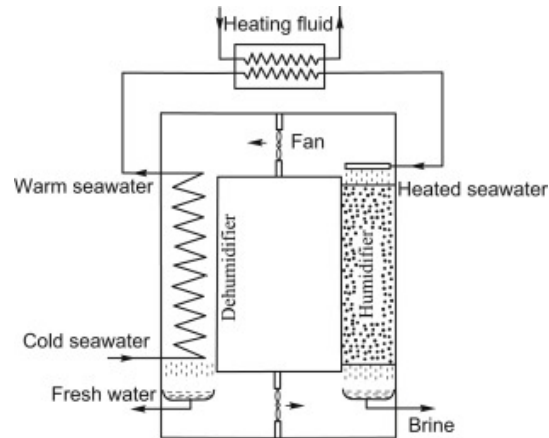


Figure 1.9: Humidification-Dehumidification desalination system. [13]

HDH systems have many advantages and are able to work in hybrid configurations with other desalination techniques, such as RO [15].

In Figure 1.10 is shown an overview of desalination technologies and their size of application compared to their GOR, that can be calculated as the ratio between the latent heat needed for the evaporation of the water produced and the energy input required by the system [16].

At the moment HDH systems need to be improved to be competitive on the large scale market.

1.2.2 Energy and environmental impacts of desalination plants

Desalination of seawater is, at present, the predominant technology used to reduce the problem of water shortage, mainly in coastal region, but not only. However this method presents some drawbacks that can be related in general to the desalination processes or, in some cases, to a specific technology.

In literature there are lots of publications about the potential impacts of desalina-

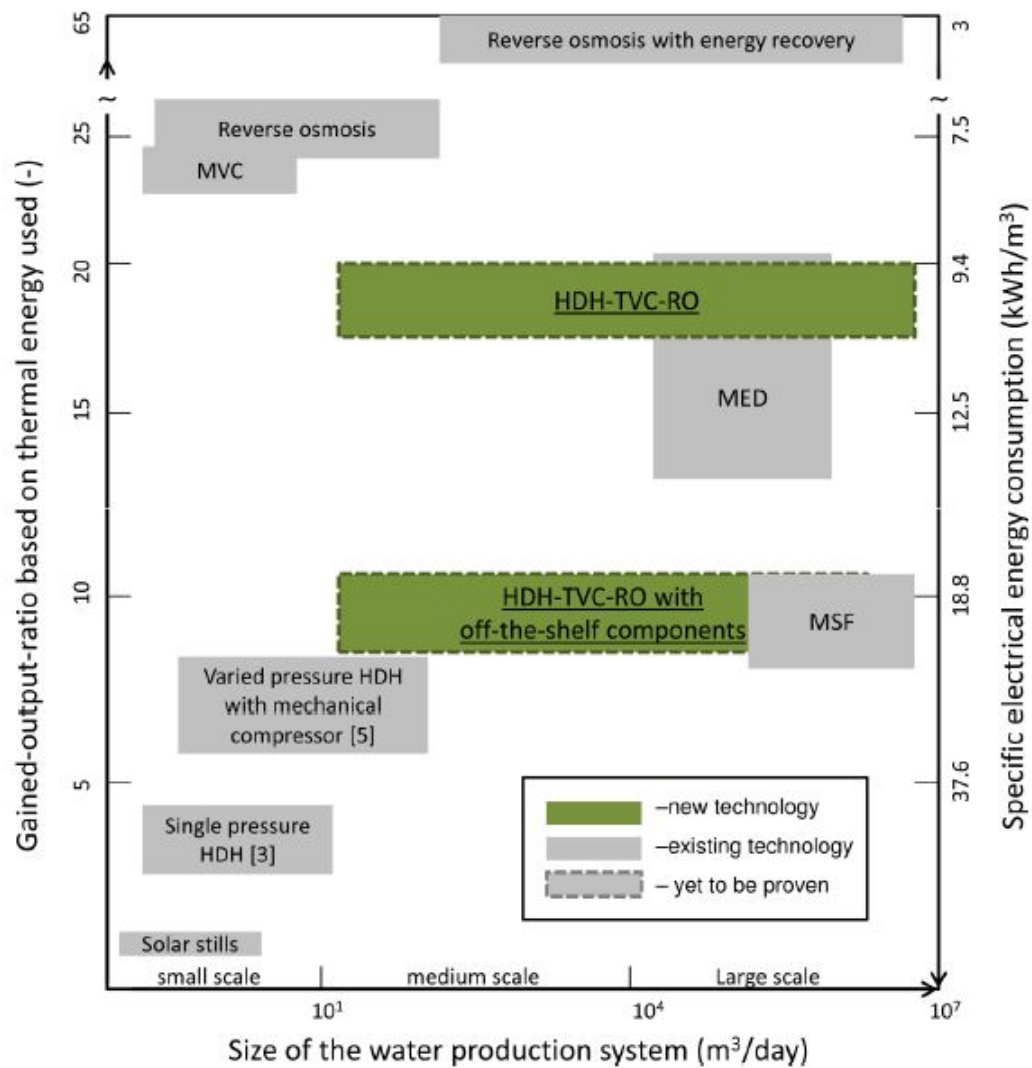


Figure 1.10: [15]

tion plants related to marine or terrestrial environment [11][17][18][19].

Nevertheless there are limits regarding the long-term effects of desalination plants. Mainly, negative impacts, are attributed to concentrate and chemical discharges, which may generate issues of water quality affecting marine life, and to the emission of pollutants and greenhouse gasses linked to the energy demand of the process. This latter problem is caused by the majority of the installed plants all over the world that are fossil-fuel based. In order to reduce this problem, desalination

processes can be coupled with renewable energy sources(solar, wind, geothermal, etc...). Also in these cases the carbon footprint problem is not totally overcome. As a matter of fact, the plants require a constant energy supply, so usually the intermittent power produced with renewable energies is directly injected into the grid.

The other main issue, as sad before, regarding the installation of these technologies along coastal areas is the potential impact on the marine environment. Firstly desalination plants can receive seawater from different sources but, in most of the cases, open seawater intakes are used. In these cases losses of aquatic organism may occur due to two reasons: they can collide with intakes screens or they can enter into the system with the water source. Then a second problem is linked to the rejected streams. In fact desalination processes produced large amount of waste water, which may increase the environment temperature, increasing also the salt concentration and, in addition, they may inject into the sea residual of pre-treatment and cleaning chemicals, and residuals due to corrosion.

Beyond these issues, that are continuously studied from many institutions, there is one last problem.

In fact, at the moment, desalination is considered the main solution to the water scarcity, but its cost is the major obstacle in its implementation, and there are many places where energy is too expensive to run desalination processes.

Against this background desalination of seawater cannot be the only solution to the alternative water source problem.

1.3 Water harvesting from atmosphere

As explained in the previous paragraph, desalination methods to produce fresh water are not able to solve the problem of water shortage in all regions around the world. For instance in arid regions, where even saline water is not present, other alternatives need to be used, such as transportation of water from other places or the extraction from atmospheric air.

Typically transportation through arid areas is very expensive and usually water

is produced by desalination plants, so it is linked to several issues(reported in section [1.2.2](#)).

Due to these reasons the solution of water extraction is becoming an interesting solution for the future. As a matter of fact, atmosphere contains about 12900 km^3 of fresh water, so it is considered a huge renewable alternative water source. H_2O is inside the air in the form of vapour and its percentage is linked to the atmospheric condition, temperature and pressure, and in general the amount of water for each cubic meter of air throughout the Earth goes from 4 to 25 g [\[20\]](#). The extraction of this source can be done in different ways, as a matter of fact in the last decades three main technologies were developed to process the atmospheric water vapour, as shown in Figure [1.11](#)

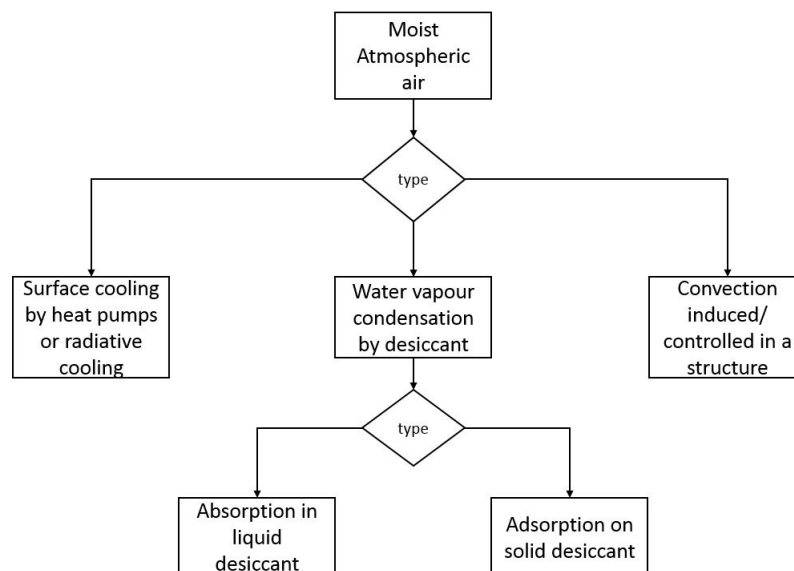


Figure 1.11: [\[20\]](#)

- The first technique is based on cool surface, made with heat pumps, in which the air is cooled under the dew point, so the water vapour condense and then is collected as liquid water. This method has the advantage that mechanical cooling is a well developed technology , but some problems can still occur

such as the freezing of the condensed vapour or the reduction of the airflow due to elements blocked by frost.

- The second solution is based on the usage of desiccants, solid or liquid. They are able to induce and maintain a state of dryness, attracting the water molecules towards their surface. Are mainly used solid adsorbent because they do not change chemically or physically. In particular materials with the best characteristics are Silica gel, Activated carbon, Activated alumina and Zeolite.
- Finally the third method is based on the control of convection in a structure, as a tower, in order to cause an expansion of air particles reducing the air temperature below the dew point. In this way water vapour condenses and precipitates as liquid. Actually, this configuration is the less studied as a possible solution for the future because is the more complex and the other two technologies have demonstrated in the last decades that can be a concrete source to produce water that only need to be improved. Thus for some reasons this third technology is less developed respect to the others that are already object of research activities^[20].

Chapter 2

Water Harvesting Cycle

The extraction of water from atmospheric air as new alternative source of water, for several regions in which, in the future, a problem of water scarcity can occur, is already a certainty.

As a matter of fact, at research level, in the last years several prototypes were born in order to make real different technologies that were introduced at the end of the twentieth century. In particular starting from different theoretical proposals nowadays the more concrete alternatives to extract water from atmospheric air are: a refrigeration cycle working with heat pumps or absorption chillers in order to cool the air under the dew point [\[21\]](#) or a thermodynamic cycle using adsorption materials in order to collect water vapour. In particular in this work is presented a system that is based on the second approach, that, in more detail, it is a machine that works with solid desiccant in order to extract water vapour from air.

This prototype was created in the laboratory of the energy department of Politecnico di Torino, and it is illustrated in [Figures 2.1](#).

This machine was tested both with silica gel grains and a zeolite coating.

2.1 Thermodynamic cycle

The prototype, presented in the previous paragraph, is based on adsorption/desorption cycles in which it firstly collects the moisture from the air and then it releases the



Figure 2.1

vapour in a controlled air flow in order to condense it as liquid water. Looking at the thermodynamic of this system, the first important consideration is that the adsorption and desorption processes are isenthalpic, so the variation of the temperature and the moisture content are strictly linked. In particular, when the moisture content is reducing, due to the adsorption of water molecules on the surface of the desiccant, the water latent heat of vaporization is released so the temperature increases. On the contrary, during desorption, the temperature decreases due to the subtraction of the latent heat necessary to regenerate the sorbent. This behaviour can be highlighted analysing the psychrometric diagram, as shown in Figure [2.2](#).

In this example it is observable that to produce a condensing stream at 35°C , the saturation point is 36.5 g/kg . So to have saturation points higher compared to the point 3, having to follow the isenthalpic line of the desorption process, the starting air temperature needs to be around 50°C and the moisture content has to be the same. The problem in this configuration is that the moisture content at the saturation is very low so condensing the vapour it is possible to produce only a small quantity ($4\text{-}5 \text{ g/kg}$).

A possible solution to improve the behaviour of the system, producing a larger amount of water, is to follow an isothermal line during the desorption transfor-

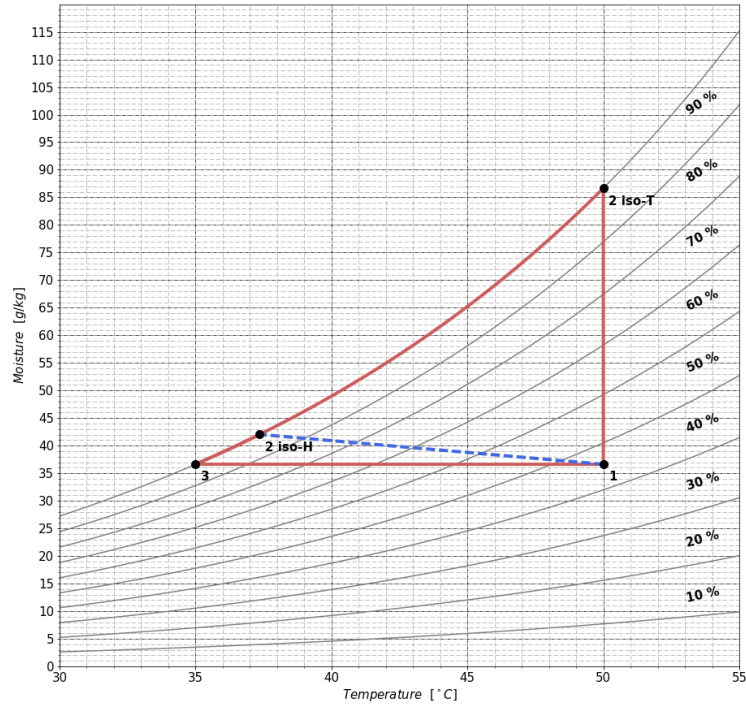


Figure 2.2: isenthalpic vs isotherm behaviour [\[22\]](#)

mation, that in [Figure 2.2](#) is represented with the line 1→2iso-T. In this way the condensing vapour is more than 40g that is significantly higher with the previous case based on the isenthalpic configuration.

In more detail, the second isothermal behaviour is able to produce more water but this is related to an higher supply of energy to permit to the water molecules to go from the desiccant to the air flow. This quantity of heat that the system needs is closer to the heat of evaporation of water multiplied by the moisture content difference. However this configuration presents significant advantages, indeed the heat supplied to the system to obtain the point 2iso-T is at the same temperature, that in this case is 50°C. On the contrary to reach the same point with an isenthalpic process the heat supply temperature would be above 70°C.

This behaviour permits to the system to work with heat at low temperature so it is possible to use, as energy source, solar collectors such as flat plate or evacuated tube or waste heat coming from several industrial processes. In that way the system is more compatible to work in arid climates, where the problem of water shortage is more relevant and typically are areas in which the solar radiation is very high and sufficient to provide enough energy to the whole machine^[22].

2.2 Prototype configuration

The main goal of the prototype that was assembled in the laboratory of the energy department of Politecnico di Torino is to extract water from atmospheric air, providing that the water contained in the atmosphere can be exploited as a new alternative source of water. The system can work alternating two different phases that are:

- Adsorption: adsorption materials are used in order to collect the water vapour contained in the atmospheric air.
- Desorption: adsorption material are heated in order to release the amount of water collected during the adsorption process.

An overview of the operating scheme is presented in Figure^[2.3].

Adsorption

During the adsorption phase the machine exchanges air with the external environment so it works as an open system. In more detail, the prototype takes an amount of air from the environment, characterized by a certain temperature and a certain moisture content. Then the air flows through the HX-ADS where its temperature is typically reduced, thanks to the water recirculation that usually is around 20°C. In addition, the water molecules inside the air are subjected to adsorption and are collected in the solid desiccant located inside the heat exchanger. The air at the end of the adsorption heat exchanger exits as dried air with a temperature close to the recirculating water temperature. Then it can be directly fed

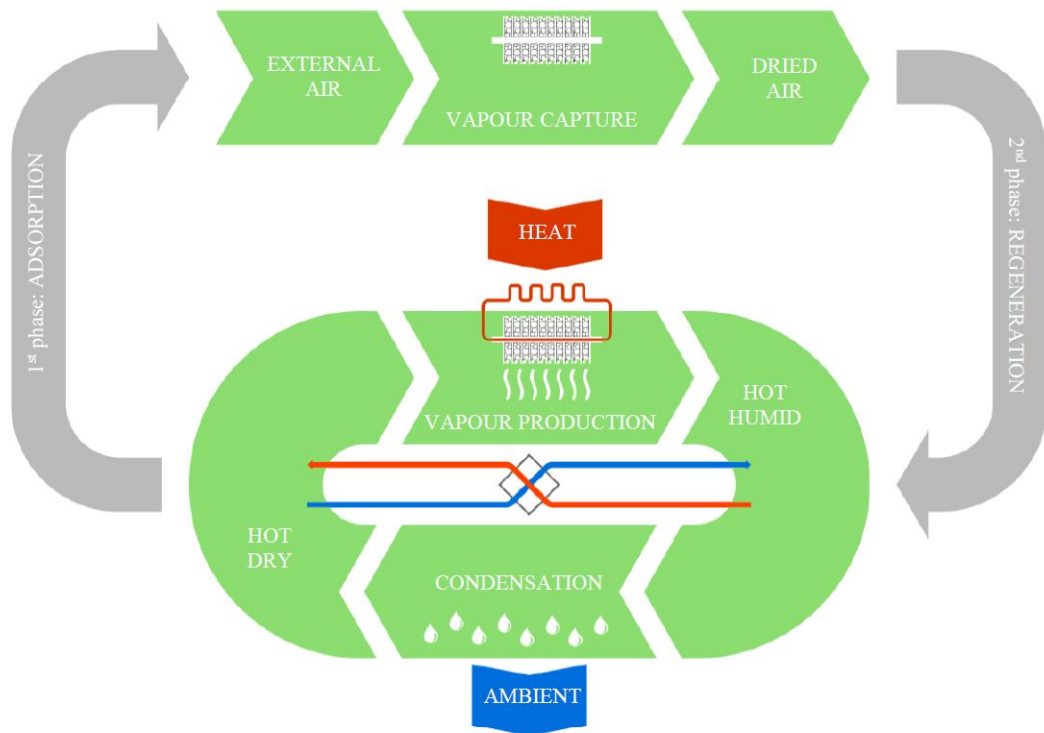


Figure 2.3: Scheme of adsorption/desorption cycle ^[22].

back to the environment.

Finally, at the end of the adsorption process the heat exchanger is loaded with a certain amount of water that depends on several factor such as the inlet moisture content, the recirculating temperature, the inlet temperature, the duration of the adsorption cycle, etc.

Desorption

The second phase of the cycle is the desorption, defined as the regeneration of the desiccant, in which the HX-ADS is heated in order to release the amount of moisture collected during the adsorption process.

The main difference between the adsorption and the desorption phase is that in the latter the system works as a closed system, with no mass exchanges with the external environment.

As a matter of fact, as shown in Figure 2.3, the air enters in the adsorption heat exchanger and then into a dry cooler where exits as hot and dry air, usable again in the HX-ADS. In the heat exchanger the hot source is the water that flows into the pipes and its temperature is typically from 50 to 80°C. This amount of heat can be produced with solar collectors, but for the experimental test can be used also an electric resistance.

Thanks to the heat supplied to the system the adsorption material releases the moisture content to the air that at the outlet is hot and humid. This air flow permits to condense the water using a dry cooler at ambient temperature.

Hence, in the condenser the water is collected as liquid and can be extract as product of the cycle. Then the hot and dry air flows again in the HX-ADS restarting the loop.

2.3 Adsorption Heat Exchanger

The main goal of the prototype is to perform the adsorption/desorption cycles following isothermal processes and to do that the system needs to exchange heat and mass at the same time. Practically it can be done using an HX-ADS that is a finned heat exchanger in which pipes for water recirculation are present, and inside the fins an adsorption material is insert, for instance, in form of grains or coating, as illustrated in Figure 2.4.

This type of operation was studied mainly for solar DEC technology [23] and also in this case the same considerations can be done.

Firstly during the adsorption phase the adsorption material releases an amount of heat heating the air flow that pass through the fins and a consequently reduction of moisture capture occurs. As a matter of fact, looking at isothermal curves of a generic adsorption process, it is evident that at higher temperature the bed humidity decreases, so, in practise, the amount of water that can be captured by the desiccant is lower. This behaviour is shown in Figure 2.5.

The presence of pipes in which water flows permits to subtract the amount of heat that the process generates keeping the fins and the air flow at a lower

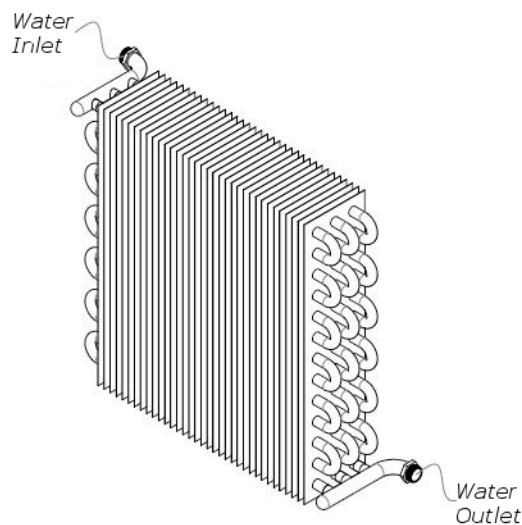


Figure 2.4: Scheme of a finned heat exchanger.

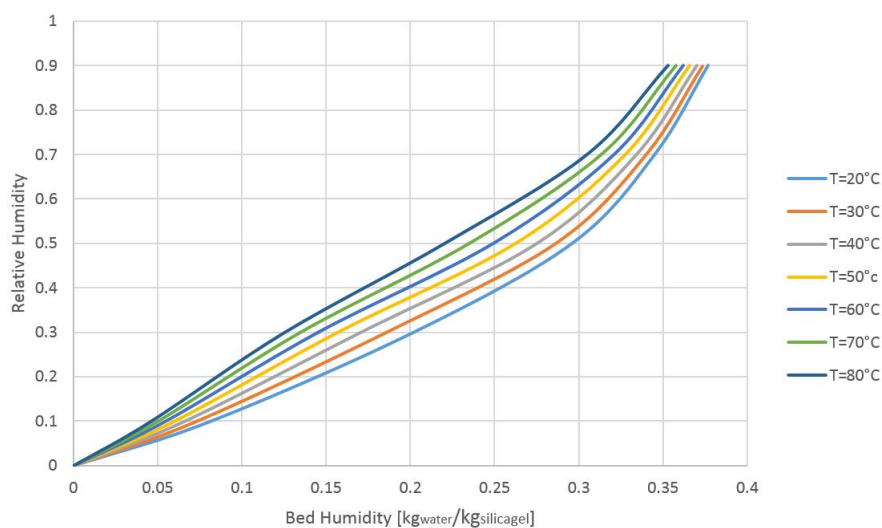


Figure 2.5: Literature data for isothermal family curves of a Silica gel [\[24\]](#).

temperature. In detail, the cooling process permits to remove a residual heat of regeneration and the adsorption heat, working at 10-20°C lower compared to a configuration without water recirculation.

This reduction of temperature increases the performance of the system during the

adsorption process.

A scheme of a cooled packed bed working with silica gel spheres is shown in Figure 2.6.

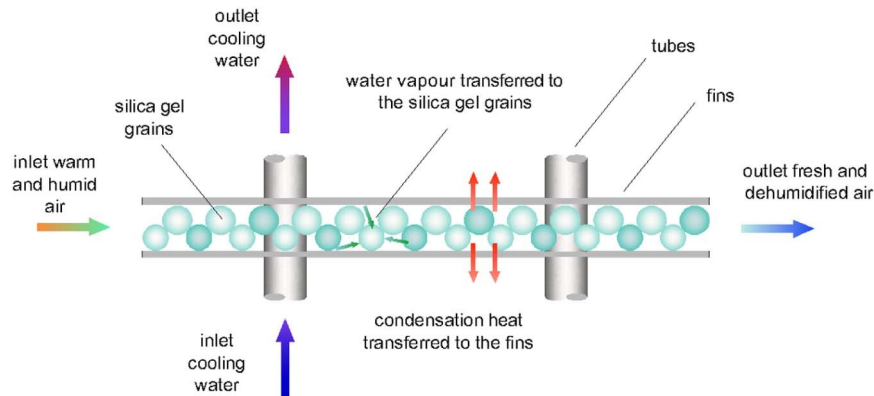


Figure 2.6: Operating scheme of a HX-ADS during adsorption [23].

Another advantages using water recirculation is during the regeneration. The inlet air flow can be injected at ambient temperature, or just a little bit higher, because the release of water from the adsorption material is guaranteed thanks to the heat supply from the hot water that flows into the pipes heating the fins and finally the desiccant. For this application the temperature of the water can vary from 50 to 80°C and it can be easily produced by solar technologies that work at low temperature such as flat plate or evacuated tube solar collectors.

Due to these reasons the prototype here presented works with a finned heat exchanger loaded with adsorption materials, shown in Figure 2.7

2.4 Adsorption materials

In the last decades lots of new porous solid that can be used for adsorption processes were studied. As a matter of fact in literature there are several reviews about this topic, and for our purposes we are mainly interesting in adsorption heat transformation. So far the most used family of adsorption materials for these applications are:

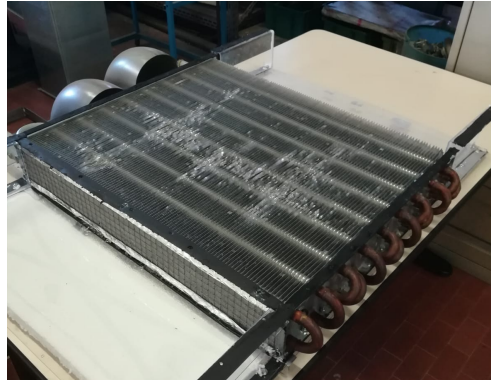


Figure 2.7: HX-ADS before being loaded with adsorption materials

- Mesoporous silicates
- Classical zeolites
- Metalaluminophosphates
- Porous coordination polymers (PCPs)
- Porous carbons
- Composite sorbents

This specific case, the material used in the adsorption heat exchanger needs to have an high capacity of adsorption and a low regeneration temperature in order to be compatible with the whole system that was developed to work mainly with solar collectors. Are now illustrated the different families of adsorption materials to shown pros and cons of each one related to this application.

Mesoporous silicates

This family of adsorption materials are mainly represented by the silica gels, that have an amorphous structure formed by aggregating primary silica particles and their specific surface area, volume and pore size are determined by the size and the packaging. Silica gel has the disadvantage that has a low sorption capacity but on the other side exhibits also some advantages. As a matter of fact, it is

cheap, stable and commercially available. Moreover, the main advantage is that it can be regenerated providing heat at very low temperature compared to other desiccants (down to 45-50°C) ^[25].

Classical zeolites

This family of desiccants covers a wide range of aluminosilicate materials. In particular, several different zeolite frameworks are known, and studied in literature ^[26] ^[27]. Changing the composition, mainly the ratio between Si and Al, the properties of water sorption vary a lot. In particular, the higher this ratio, the less hydrophilic is the zeolite.

Typically, the water affinity is very high, and then they can adsorb a large amount of water at relatively low values of relative pressure ^[25]. On the other hand, classical zeolites are not used a lot in adsorption heat transformation because they need high temperature heat for the regeneration.

In conclusion, this family of adsorption material is not suitable for our purpose.

Metalaluminophosphates

Crystalline porous phosphates have been synthesized since the 80s, and they represent the first class of framework oxides without silica ^[25] ^[28]. They have a similar structure to aluminosilicate zeolites, but they present different properties. The main difference is noted on the isotherms that permit low regeneration temperature, around 60-90°C. This makes them more usable for the application in the prototype. A disadvantage is that the synthesis is more complex, so their cost is higher compared to classical zeolites and mesoporous silicates.

In addition, their affinity to water is higher than silica gels but lower compared to aluminosilicate zeolites. To improve this property, increasing their adsorption capacity, aluminophosphates can be changed structurally by replacing various metals into the framework, such as Si, Ge, Sn, Ti, etc. The more promising family of these substituted aluminophosphate are the silicoaluminophosphate (SAPO), in which P is substituted with Si. In particular, looking for the application in heat adsorption cycle, one of the most compatible SAPO is the SAPO-34.

This adsorbent presents a structure with regular pores and a 3D-structure similar to zeolites, that generates a moderate hydrophilicity associated to an high adsorption capacity^[29]. Consequently it presents a low temperature of desorption (60-100°C) that is a very good feature for the application in the prototype^[30].

Porous coordination polymers(PCPs)

This class of materials, also called metal-organic frameworks(MOFs), is a subgroup of the coordination polymers, and they are characterized by an organized structure that presents an high porosity.

They are very promising materials thanks to their properties, such as an adaptable pore size and an high surface area, but nowadays are mainly used for for gas separation, catalysis and gas storage^[25]. As a matter of fact, even if they presents an high hydrophilicity, in general PCPs are unstable in contact with water.

The prototype presented in this work, have the goal to produce potable water, so in principle the usage of MOFs was not considered for this incompatibility.

Porous carbon

The porous carbon are activated carbons characterized by an high porosity and high surface area. They are very common as desiccants due to their cost, indeed they are very cheap compared to other adsorption materials. They are mainly produced during the char gasification.

This class of desiccant are typically used for the separation and purification of gasses and the purification of liquids. Also for cooling systems they are widely used as adsorbate liquids like methanol or ammonia^[31].

Composite sorbents

Composite sorbents include a wide range of materials that are made with salts insert in a porous matrix. Lot of different configurations were studied so far, for different operating condition. The idea is to use a porous matrix as a structure in which the salt is dispersed and the latter works as active component^[25].

For our purposes, an interesting subgroup is the class of materials that use water as sorbate. They are called Selective Water Sorbents(SWS). Also in this case there is a porous matrix , e.g. silica gels, in which an hygroscopic salt is inserted into its pores, in order to increase the adsorption properties. An example of SWS material is $CaCl_2$ confined into silica gel. These families of composite sorbents are very promising because they are characterized by an high capacity of water sorption and they can be used for several applications.

For instance, they were studied in application fields such as: gas drying, refrigeration machines, thermal insulation, cooling of electronic devices, air conditioning, etc [32](#). In particular they are interesting also for water production from atmospheric air.

So far, different families of adsorption materials are presented, analysing also their operating fields. In particular, for the application of water extraction from atmospheric air, the adsorption material has to work in the HX-ADS. For this reason, it is necessary to study the dynamic of adsorption of these materials applied to this specific configuration, in order to choose the most compatible desiccant. Starting from the structure of the adsorption heat exchanger, in literature, two main configurations are defined:

- a) Finned heat exchanger with a coating of adsorbent material.
- b) Finned heat exchanger in which the void between the fins is filled with sorbent grains.

The first layout can be done in two different ways.

In situ, when the adsorption material is directly deposited on the surface of the fins, or *ex situ*, when to fix the desiccant a binder layer is used. The latter configuration presents some drawbacks because the binder layer reduces a lot the mass transfer so the adsorption process is penalized. Mainly for this reason, the *in situ* configuration is the most used for adsorption heat exchanger configurations. As a

Structure	Water capacity* [g/g]	Surface area [m^2/g]	Pore volume [cm^3/g]	Particle size [μm]
CHA	$\geq 0.30-0.32$	≥ 550	≥ 0.27	~ 2

*100% humidity, at 25°C.

Table 2.1: Adsorbent properties [\[30\]](#)

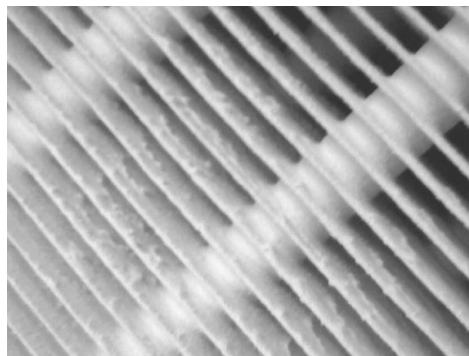


Figure 2.8: fins coated with SAPO-34 zeolite

matter of fact, the first HX-ADS assembled in the laboratory is made with a zeolite coating with an *insitu* synthesis.

In more detail, a SAPO-34 zeolite was selected for the coating. The choice of this type of desiccant was carried out for the excellent adsorption properties and for the possibility to regenerate it with low temperature heat.

An overview of the SAPO-34 properties is presented in Table [2.1](#), and a detail of the HX-ADS is illustrated in Figure [2.8](#).

On the other hand, the second layout(b), is very simple to realize compared to the coating procedure because it is made only with spheres of desiccants loose inside the fins. This configuration typically is characterized by an excellent vapour transport but presents some problems with the heat transfer. Indeed, the thermal resistance between the fins and the adsorbent spheres is usually very high so the heat transfer is lower and the sorption kinetic too [\[25\]](#). Another important difference in the two configurations is the ratio between the adsorption surface area and the pressure drop.



Figure 2.9: Finned heat exchanger in which the void between the fins is filled with silica gel grains.

In more detail, the first configuration, with the coating, the pressure drops inside the HX-ADS are lower compared to the configuration (b) but consequently the surface of adsorption is lower. In the configuration with silica gel grains the problem is the opposite: an higher surface of adsorption is available but also an higher pressure drop inside the adsorption heat exchanger is present.

In order to test both configurations also a finned heat exchanger with filled with grains of desiccant is used for test the prototype. The second HX-ADS is shown in Figure 2.9.

In this case, as mentioned before, a composite sorbent, in particular SWS, is more performing because with the same surface area it is able to collect an higher amount of water.

For example, in a water adsorption application, a possible solution can be the usage of silica gel grains in which $CaCl_2$ is added inside the pores.

Obviously the price of a SWS compared to simple silica gel is higher so, in this case, for initial tests the HX-ADS was loaded with pure silica gel grains, without any salt inside.

2.5 Geometry optimization

As presented so far, the adsorption heat exchanger covers an important role in the prototype operation. As matter of fact, a lot of variables of the whole system are related to this component, such as the amount of water collected, the energy consumption and so the efficiency.

Considering the efficiency of the machine as the water produced per unit of energy required, some considerations can be done. As a matter of fact, one of the main problem related to the adsorption heat exchanger is the relation between the pressure drop and the active surface area for the adsorption. These two quantities are strictly linked together because an higher adsorption area means higher pressure drop and vice versa. However to maximize the efficiency the system has to work with high surface area and low pressure drop.

Indeed, high pressure drops mean that the energy consumption for recirculating the air increases so the whole requirements of energy becomes higher and the total efficiency decreases.

On the other hand, low surface area for adsorption means that the system is able to collect a lower amount of energy per unit of time so the efficiency is reduced. Different configurations of the adsorption heat exchanger can be considered and a series of tests can be performed in order to understand what is the best compromise between pressure drop and adsorption surface area. The problem of these approach is related mainly with the costs and the time required to tests different configurations.

An alternative solution to avoid these issues is to create a CFD(Computational fluid dynamics) model of the adsorption heat exchanger in order to test different configurations with CFD simulations. In this way is possible to reduce both costs and time for simulating different geometry. Moreover, with a valid model, is possible to test not only the geometry but also different adsorption material, with different configurations, such as coating or grains. In addition, adsorption/desorption cycles can be performed analysing different operating conditions such as different air temperatures, water temperatures, different ambient conditions, etc.

To do that an adsorption model has to be defined in order to simulate with a CFD

software this phenomenon and then must be validated on experimental data. The goal of this work is to present an adsorption model valid for the simulation of the adsorption heat exchanger used in the prototype.

To do that a CFD software is used: STAR-CCM+.

Chapter 3

Introduction to CFD

The Computational Fluid Dynamics (CFD) is the analysis of systems regarding fluid flow, heat transfer, chemical reactions and other phenomena, done with computer simulations. This method is very useful to model real systems and can be used to study a wide range of cases. [\[34\]](#).

Initially, in the '60, CFD techniques were used mainly for the aerospace industry, while currently is applied for a lot of industrial and non-industrial fields, such as:

- Chemical processes
- Power plants
- Hydrodynamics
- Thermal comfort
- Meteorology
- Marine engineering
- Aerodynamics of vehicles
- Biomedical engineering

As a matter of fact, today the availability of high performances computing hardware allowed the development of engineering software that permit to use CFD

for research activities or for industrial design. Comparing the experimental-based approach compared to CFD there are several advantages such as the reduction of time and costs for design, the possibility to control experiment that in the reality are difficult or not performable, the ability to study hazardous condition without any risk and finally the practically unlimited availability of results.

The market of CFD software is dominated principally by four programs that are STAR-CD, PHOENICS, FLUENT, FLOW3D and they are based on finite volume method that can be described with the following steps:

- Integration of dominant equations of a fluid flow upon each finite control volume of the domain.
- Discretization, that implies the replacement of finite-different-type approximations for the terms representing the flow processes such as diffusion, source and convection, in the integrated equation. It consists in the convection of integral equations into a system of algebraic equations.
- Using iterative methods to solve the algebraic equations.

In addition, all CFD software provide a detailed interface, to allow easy access to all their computational features.

3.1 CFD code structure

All CFD codes follow the same structure and they can be divided in mainly 3 elements : a pre-processor, a solver and a post-processor.

3.1.1 Pre-processor

This step is about inserting input data of a certain flow problem in a CFD tool by means of a user-friendly interface and the consequent transformation of these data into a suitable form for the following element: the solver.

In more detail is done by the following stages:

1. Definition of the domain, introducing the geometry of the model.
2. Mesh-generation: division of the domain into a number of smaller, non-overlapping cells.
3. Selection of the phenomenon, physically or chemically, that has to be modelled.
4. Definition of the properties of the fluid.
5. Definition of the pertinent boundary conditions over the cells located at the domain boundary.

The precision of the solution is strictly linked to the number of cells in the grid. As a matter of fact the solution of flow problem, in terms of velocity, pressure, temperature, etc. is defined at nodes inside each cell.

. Typically the best meshes are non-uniform: finer where more complex variations occur in nearby points and coarser where the solution is subjected to little changes.

3.1.2 Solver

There are different solution techniques but all these numerical methods are based on the following steps:

- Unknown flow variables are approximated by means of simple functions.
- Discretization of the governing flow equations, substituting the approximations.
- Algebraic equations are solved.

The different solution techniques differ mainly in the discretization process changing the way in which the flow variables are approximated.

As said before, the most used software use the method of finite volume.

3.1.3 Post-processor

In the last few years, workstations with excellent capabilities become more common and their use is increasing, as result CFD software are now equipped with versatile data visualization tools. For instance, with a software we are able to display the geometry of the domain and the mesh, we can do vector plots or plotting 2D and 3D surfaces. It is also possible to track the particles motion, colour postscript output and manipulate views with transformations such as translation, rotation, scaling, etc.

Nowadays thanks to the development of graphics tools is possible to edit animation for dynamic results^[34]. All these improvements have allowed greater sharing, even to non-specialist people.

In a CFD simulation is crucial to understand the goodness of the numerical solution. To do that it is important to know the algorithm that the software uses for solving the problem. Three concepts are helpful in determining the success of the algorithm: convergence, consistency and stability.

“Convergence is the property of a numerical method to produce a solution which approaches the exact solution as the grid spacing, control volume size or element size is reduced to zero. Consistent numerical schemes produce systems of algebraic equations which can be demonstrated to be equivalent to the original governing equation as the grid spacing tends to zero. Stability is associated with damping of errors as the numerical method proceeds. If a technique is not stable even roundoff errors in the initial data can cause wild oscillation or divergence.”^[34]

Typically is very difficult to verify the convergence of a solution, so in practise we rely on the Lax’s equivalence theorem. It asserts that for linear problems, the verification of the stability and consistency of the method is a necessary and sufficient condition for convergence. When we are dealing with non-linear problems the fact that it is stable and consistent is a necessary condition for convergence, but not sufficient^[34].

3.2 Fluid dynamics equations

The three main equations that govern the fluid flow are the representation of the conservation laws in physics³⁴.

- The law of conservation of mass.
- The second law of Newton: the rate of change of momentum of a body is directly proportional to the force applied, and this change in momentum takes place in the direction of the applied forces.
- The first law of thermodynamic: the increase in internal energy of a closed system is equal to the total of the energy added to the system.

In this representation we consider the fluid as a continuum, analysing the behaviour of an element of fluid with macroscopic properties, such as pressure, temperature, density and velocity. In more detail the analysis of a fluid particle is done ignoring the molecular structure of the matter and the molecular motion.

3.2.1 Conservation of the mass

At first, we have to write the mass balance for the fluid element, that can be described as:

$$\boxed{\begin{array}{c} \text{Rate of increase of} \\ \text{mass in fluid} \\ \text{element} \end{array}} = \boxed{\begin{array}{c} \text{Net rate of flow of} \\ \text{mass into fluid} \\ \text{element} \end{array}}$$

Considering the infinitesimal control volume we integrate the differential equations over the system in order to obtain local conditions.

In Figure^{3.1} are shown the dependent variables (u,v,w,ρ) as a function of the independent variables (x,y,z,t) .

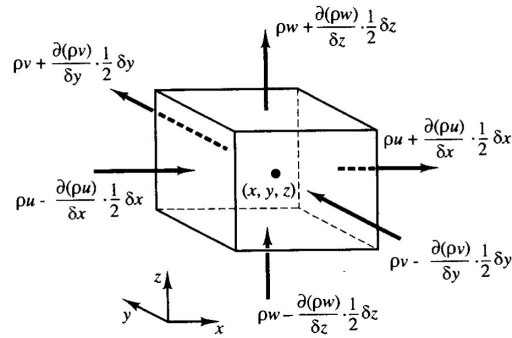


Figure 3.1: Mass flows of the fluid element. [324](#)

Where:

- u is the velocity along the x -axis.
- v is the velocity along the y -axis.
- w is the velocity along the z -axis.
- ρ is the density.

Taking into account one single direction (x) it is possible to write :

$$\rho u dx dy dz dt = \left(\rho u + u \frac{\partial \rho}{\partial x} dx + \rho \frac{\partial u}{\partial x} dx \right) dy dz dt + \frac{\partial \rho}{\partial t} dx dy dz dt \quad (3.1)$$

where the left hand side is the entering term while the right hand side is the sum of the exiting and the accumulated terms.

Extending this equations along all directions (x, y, z) it can be written in a more compact way the rate of mass change inside the control volume equal to the net rate of flow of mass into the fluid element across its faces:

$$\frac{\partial(\rho u)}{\partial x} + \frac{\partial(\rho v)}{\partial y} + \frac{\partial(\rho w)}{\partial z} = -\frac{\partial \rho}{\partial t} \quad (3.2)$$

In a vector notation becomes:

$$\text{div}(\rho \mathbf{V}) = -\frac{\partial \rho}{\partial t} \quad (3.3)$$

In case of incompressible fluid, like a liquid, the density is constant so results:

$$\text{div}(\rho\mathbf{V}) = 0 \quad (3.4)$$

3.2.2 Momentum equations

The balance of the momentum on the fluid element can be defined as:



Firstly we can consider the increase of x,y,x momentum per unit of volume as:

$$\rho \frac{Du}{Dt} ; \rho \frac{Dv}{Dt} ; \rho \frac{Dw}{Dt} \quad (3.5)$$

Then the forces applied on the fluid element can be divided in two different classes:

- Surface forces, such as the pressure and the viscosity.
- Body forces, that include the gravity, the Coriolis force, the centrifugal forces, etc.

Typically in the momentum equations the contribution of the surface forces is highlighted as separate terms while the body forces are considered all together in the source term.

In this case we consider the state of stress of a fluid element by means of pressure and the nine viscous stress components, that are shown in Figure 3.2.

We define p as the pressure, while viscous stresses are denoted as τ . P acts on the direction normal to the surface, on the contrary τ is applied on different directions that in are defined by the different suffix notation. j is the direction on the surface normal to the i -direction.

Including the body forces as part of the source terms , S_M , we can write the

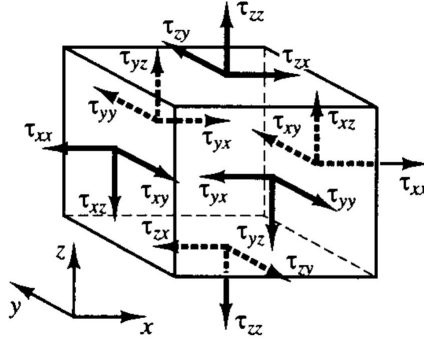


Figure 3.2: Stress components of the fluid element. [34](#)

x-component of the momentum equation as the sum of the total force in the x-direction over the control volume due to surface stresses and the rate of increase of the x-momentum caused by the source, equal to the rate of increase of the momentum of the fluid infinitesimal volume:

$$\rho \frac{Du}{Dt} = \frac{\delta(-p + \tau_{xx})}{\delta x} + \frac{\delta \tau_{yx}}{\delta y} + \frac{\delta \tau_{zx}}{\delta z} + S_{Mx} \quad (3.6)$$

In the same way we can define the y and z components of the momentum equation as follow:

$$\rho \frac{Dv}{Dt} = \frac{\delta \tau_{xy}}{\delta x} + \frac{\delta(-p + \tau_{yy})}{\delta y} + \frac{\delta \tau_{zy}}{\delta z} + S_{My} \quad (3.7)$$

$$\rho \frac{Dw}{Dt} = \frac{\delta \tau_{xz}}{\delta x} + \frac{\delta \tau_{yz}}{\delta y} + \frac{\delta(-p + \tau_{zz})}{\delta z} + S_{Mz} \quad (3.8)$$

3.2.3 Energy equations

Considering the rate of increase of the energy(E) of a fluid element per unit of volume as:

$$\rho \frac{DE}{Dt} \quad (3.9)$$

And the total increase of work done on the fluid element by surface stresses:

$$\begin{aligned}
- \operatorname{div}(\rho \mathbf{u}) + \frac{\delta(u\tau_{xx})}{\delta x} + \frac{\delta(u\tau_{yx})}{\delta y} + \frac{\delta(u\tau_{zx})}{\delta z} + \frac{\delta(v\tau_{xy})}{\delta x} \\
+ \frac{\delta(v\tau_{yy})}{\delta y} + \frac{\delta(v\tau_{xz})}{\delta z} + \frac{\delta(w\tau_{yz})}{\delta x} + \frac{\delta(w\tau_{xz})}{\delta y} + \frac{\delta(w\tau_{zz})}{\delta z} \quad (3.10)
\end{aligned}$$

And finally introducing the Fourier's law to describe the rate of heat increase on the fluid particle due to heat conduction:

$$- \operatorname{div}(\mathbf{q}) = \operatorname{div}(k \operatorname{grad}T) \quad (3.11)$$

Where:

- k is the thermal conductivity
- T is the temperature

We can write the energy equation as the combination of these terms.

In more detail, the energy can be considered as the sum of internal energy, kinetic energy and potential energy. In this analysis the potential term is considered as a body force, presented in previous paragraph, so it is included in the source term. We highlight it separating this term, S_E , in the equation as a source per unit of volume per unit of time.

In conclusion the equation of conservation of energy can be reassumed as the rate of increase of the energy of the fluid particle equal to the sum of the other terms: the net rate of work done on the fluid volume, the net rate of heat addition to the particle and the rate of change due to external forces [\[34\]](#).

$$\begin{aligned}
\rho \frac{DE}{Dt} = - \operatorname{div}(\rho \mathbf{u}) + \frac{\delta(u\tau_{xx})}{\delta x} + \frac{\delta(u\tau_{yx})}{\delta y} + \frac{\delta(u\tau_{zx})}{\delta z} \\
+ \frac{\delta(v\tau_{xy})}{\delta x} + \frac{\delta(v\tau_{yy})}{\delta y} + \frac{\delta(v\tau_{xz})}{\delta z} + \frac{\delta(w\tau_{yz})}{\delta x} + \frac{\delta(w\tau_{xz})}{\delta y} + \frac{\delta(w\tau_{zz})}{\delta z} \\
+ \operatorname{div}(k \operatorname{grad}T) + S_E \quad (3.12)
\end{aligned}$$

Chapter 4

Adsorption model with STAR-CCM+

Typically in CFD software there are no default models that performed the adsorption phenomenon. Otherwise, in some software, it can be modelled with electrochemical models that describe the physics of the phenomenon but using them for simulate whole components requires an high computational time.

For this reason, the goal of this work is to produce a quick CFD model that describes the adsorption phenomenon and the heat and mass transfer inside a HX-ADS, finalized to simulate the prototype presented in the chapter [2](#).

In particular, the model has to recreate the phenomena that occur inside the adsorption heat exchanger for each type of configuration we want to test.

In more detail, starting from quantities that a CFD software typically calculates, a set of equations and additional variables must be added. To do that, a model of theoretical equations has to be defined in order to evaluate the heat and mass transfer between the air and the adsorption material. Then it has to be implemented on the software. The idea is to insert, in STAR-CCM+, the set of equations as scalar *Field functions* that each iteration are solved for each cell, evaluating the mass flux that flows through the desiccant.

This allows, with a relatively low computational cost, to solve the system of new variables and consequently to described the physics phenomena that characterize

the adsorption heat exchanger.

In particular, the model was developed starting from a configuration of a finned heat exchanger loaded with silica gel grains loose in the room between the fins. The model has been validated against experimental data of a similar configuration tested in laboratory of Energy Department of Polytechnic of Turin. The physical phenomena occurring in the silica gel packed bed, such as adsorption, heat and mass transfer, has been simulated with the software STAR-CCM+.

4.1 Model description

Two hypothesis were done for the definition of the model:

- In the neighbouring area of the adsorbent surface a quasi-instantaneous thermodynamic equilibrium condition occurs. This occurs because the adsorption process is much faster compared to other phenomena such as the water vapour diffusion through pores of the adsorption material.
- The heat generated by the adsorption is located on the surface of the silica gel and it is transferred to the air as a specific flux [W/m^2]. In more detail, it was considered as constant and equal to the heat of vaporization on a the operating water partial pressure range ($H_{ads} = 2500[kJ/kg]$).

Starting from these hypothesis, the model is made of a set of equations that are applied on the surface of the adsorption material and the software solved the equations for each time step for each cell according to the mesh operation made in the pre-processing.

The mass flux on the desiccant surface is determined by the difference between the vapour partial pressure and the same value in the equilibrium condition. It can be written as^[33] :

$$\dot{m}_{H_2O} = -\frac{D_{H_2O} \cdot (p_v - p_{eq})}{R \cdot T} \cdot A \quad [kg/m^2 \cdot s] \quad (4.1)$$

Where:

- D_{H_2O} is the effective coefficient of diffusion of water in silica gel
- p_v is the vapour partial pressure of vapour air mixture
- p_{eq} is the vapour partial pressure of air mixture in the equilibrium condition with silica gel moisture content.
- A is a global coefficient that accounts for the molecules mass of water and the main average pore dimension
- R is the ideal gas constant

p_v and p_{eq} are calculated as follows:

$$p_v = \frac{x \cdot p_a}{0.622 + x} \quad [Pa] \quad (4.2)$$

$$p_{eq} = \frac{x_{eq} \cdot p_a}{0.622 + x_{eq}} \quad [Pa] \quad (4.3)$$

Where:

- p_a is the ambient pressure, considered constant and equal to 101325 Pa.
- x is the moisture content of the vapour air mixture defined as [kg of vapour/kg of air].
- x_{eq} is the equilibrium air moisture content defined as [kg of vapour/kg of air].

x and x_{eq} can be evaluated as:

$$x = 0.622 \cdot \frac{RH \cdot p_{v_{sat}}}{p_a - RH \cdot p_{v_{sat}}} \quad (4.4)$$

$$x_{eq} = 0.622 \cdot \frac{RH_{eq} \cdot p_{v_{sat}}}{p_a - RH_{eq} \cdot p_{v_{sat}}} \quad (4.5)$$

Where 0.622 coefficient is given by the ratio between gas constant of air and water vapour. $p_{v_{sat}}$ is the saturated vapour pressure expressed in $[Pa]$. RH is the air relative humidity.

RH_{eq} is the air relative humidity in equilibrium condition and depends on the temperature of the adsorption material (T_s) and on the bed humidity. The humidity of the bed is defined as W and is expressed in kg of water per kg of dry silica gel. The dependency of the air relative humidity in equilibrium condition is defined by the isotherms of a specific adsorption material.

In particular, for this application, a regression of family isotherms curves for silica gel it has been developed:

$$RH_{eq} = S_1 \cdot T_s + S_2 \cdot T_s^2 + S_3 \cdot W + S_4 \cdot W \cdot T_s + S_5 \cdot W \cdot T_s^2 + S_6 \cdot W^2 + S_7 \cdot W^2 \cdot T_s + S_8 \cdot W^3 + S_9 \cdot T_s^3 \quad (4.6)$$

The coefficients S_n have been evaluated experimentally in order to obtain a regression of specific isotherms of the silica used in the HX-ADS of the prototype. The experimental tests carried out to obtain this regression are explained in the section [4.1.1](#), where also the coefficients S_n are presented.

The software calculates directly the temperature of each cell on the surface of the silica spheres while the value of W must be set as new variable. To do that, firstly, a monitor that evaluates the total adsorbed mass of water, during the transient, for each cell is necessary. Then it is possible to define the variable W as:

$$W = \frac{Totaladsorbedmass}{\rho_s \cdot V_c} \quad (4.7)$$

V_c is the volume of adsorbent material that for each cell is available to collect water.

In this case, working with spheres, the volume was approximated as the area of a pyramid with a square base.

$$V_c = \frac{Area_{cell} \cdot R_{sphere}}{3} \quad [m^3] \quad (4.8)$$

The set of equations presented so far permits to evaluate the water mass flux between the air and the adsorption material. The input data needed to solve this set of equations are the mass fraction of water in the air, the temperature on the surface of the sorbent and the area of each cell.

Finally, also the heat exchange must be considered. To do that, as hypothesis, a constant value of heat of water vaporization equal to $2500[kJ/kg]$ has been considered. The total heat flux on the surface of the adsorbent due to adsorption, can be evaluated as:

$$\dot{q}_{ads} = -\dot{m}_{H_2O} \cdot H \quad [W/m^2] \quad (4.9)$$

As shown in the formula [4.9](#) the heat flux and the mass flux are characterized by different sign. This occurs because the two fluxes are directed in opposite directions. As a matter of fact, during adsorption, the mass flux goes from the air to the sorbent and then a heat flux is generated, so q_{ads} is directed towards the gas. On the contrary, during desorption, the water mass flux is released in the air while the specific heat flux is directed from the external to the internal of the adsorption material.

4.1.1 Experimental determination of Silica gel Isotherms

For the application of the theoretical model to obtain the heat and mass flux through the surface of a adsorbent, the family of isotherms curves of the material is necessary. As a matter of fact, isotherms permit to evaluate the air relative humidity in equilibrium condition as a function of the temperature and the moisture content of the adsorption material. Each material is characterized by a specific family of isotherms that are different for different sorbents. In addition, based on some properties of the materials, such as the hydrophilicity, isotherm curves can have different behaviours. The IUPAC classification divides adsorption isotherms in six classes, as shown in Figure [4.1](#) [35](#).

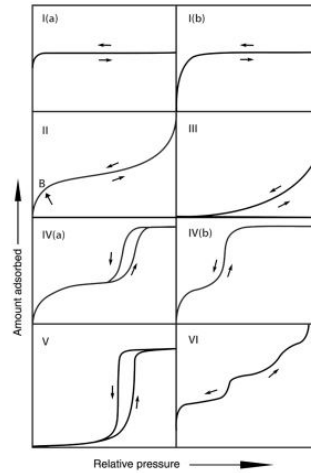


Figure 4.1: IUPAC classification of the adsorption isotherms [35](#).

In this work is presented the evaluation of the isotherms curves of the silica gel used in the adsorption heat exchanger. The measures were done using the climatic room of the Energy Department, shown in Figure [4.2](#).

A sample of silica gel grains was weighted in different conditions of temperature and relative humidity. In this specific case, at 30,40 and 50°C the sample was measured for intervals of 20% of HR starting form 10% to 90%. In addition as a dry value of the material the weighted at $T=50^{\circ}\text{C}$ and $HR = 10\%$ was used. The sample for each measure was left inside the climatic room for at least 8 hours to permit the achievement of the equilibrium condition between the silica gel and the air. In any case, the test of the single sample wasn't stopped until reaching a variation of the weight less than 0.1%. Then, after the measurements, the specific amount of water per unit of mass of the sorbent has been calculated, from the data, as:

$$W(T, HR) = \frac{W^*(T, HR) - W_{dry}^*}{W_{dry}^*} \quad [kg_{H_2O}/kg_{SiO_2}] \quad (4.10)$$

The three isotherms calculated in that way are shown in Figure [4.3](#).

After the evaluation of the experimental isotherms, a polynomial regression was calculated in order to insert it in the software for the implementation of the



Figure 4.2: Climatic room of the Energy Department of the Polytechnic of Turin.

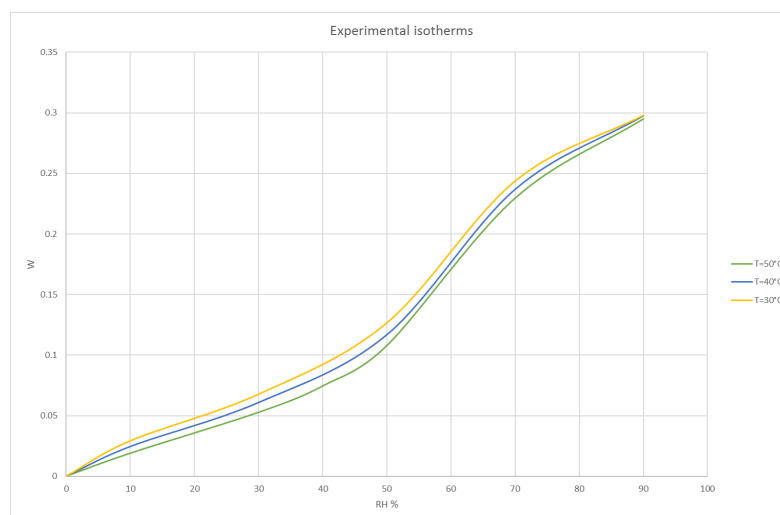


Figure 4.3: Experimental isotherms of the silica gel used for the test in the prototype

theoretical model.

To do that, a MATLAB code was used that permits to perform polynomial regression on multidimensional data [\[36\]](#). In order to achieve a good fitting of the experimental data a third order polynomial regression was carried out.

Finally, the regression of the family isotherms of the silica gel used for the CFD simulations is the formula [4.6](#). The coefficients are:

S_1	-2.26E-03	S_6	-3.87E+01
S_2	+1.28E-04	S_7	+8.63E-03
S_3	+7.96E+00	S_8	+8.15E+01
S_4	-1.15E-02	S_9	-8.56E-07
S_5	-2.07E-05		

A graphic comparison of the curves respect to the experimental data is shown in Figure 4.4. In addition, the relative error between the measurements obtained in the climatic room and the values of W resulting from the regression are shown in table 4.1.

The error is higher for low values of RH. Indeed, for RH=10% it reaches a maximum of 7% but for RH>50% it decreases under 1%. This behaviour will affect the simulation, in particular during the regeneration, where RH will be lower than in adsorption.

Finally, an additional issue must be consider in order to implement the regression in the software. In fact, as shown in Figure 4.5, the regression uses as dry value the water uptake measured at T=50°C and RH=10%, so for values at higher temperature and lower relative humidity the water uptake becomes negative.

In reality, for these values of T and RH the adsorbent is dry so its water uptake is zero. To recreate this condition in the simulation the regression was used with a constrain: when RH<0 it is set equal to zero.

Table 4.1: Relative error of the regression of the family isotherms.

RH	T [°C]	$W_{regression}$ [kg/kg]	W_{test} [kg/kg]	Relative Error [%]
0.00	30	-0.00297	0	/
0.10	30	0.0106	0.010	5.00%
0.30	30	0.0460	0.048	3.78%
0.50	30	0.1086	0.106	2.81%
0.70	30	0.2185	0.221	0.93%
0.90	30	0.2743	0.274	0.19%
0.00	40	-0.0075	0	/
0.10	40	0.0058	0.005	6.89%
0.30	40	0.0397	0.041	3.33%
0.50	40	0.0982	0.096	2.23%
0.70	40	0.2137	0.214	0.06%
0.90	40	0.2731	0.273	0.11%
0.00	50	-0.0126	0	/
0.10	50	0.0002	0	/
0.30	50	0.0326	0.033	1.49%
0.50	50	0.0866	0.87	0.74%
0.70	50	0.2061	0.207	0.31%
0.90	50	0.2710	0.271	0.05%

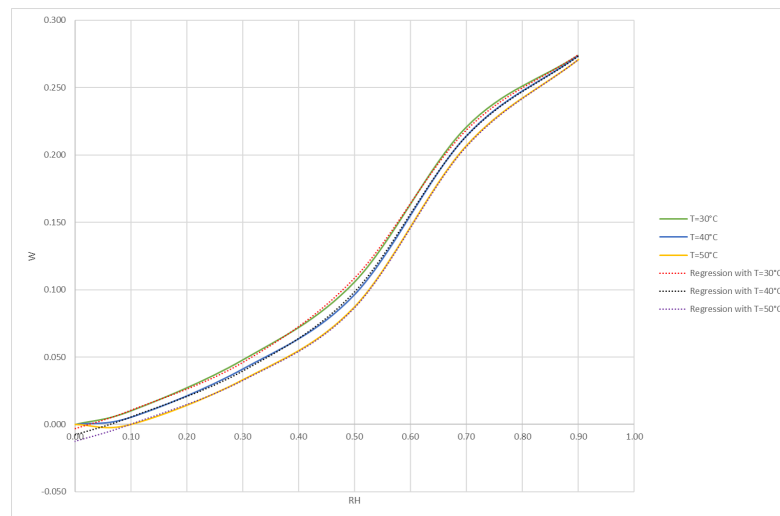


Figure 4.4: Comparison between the experimental isotherms compared to the curves obtained with the regression

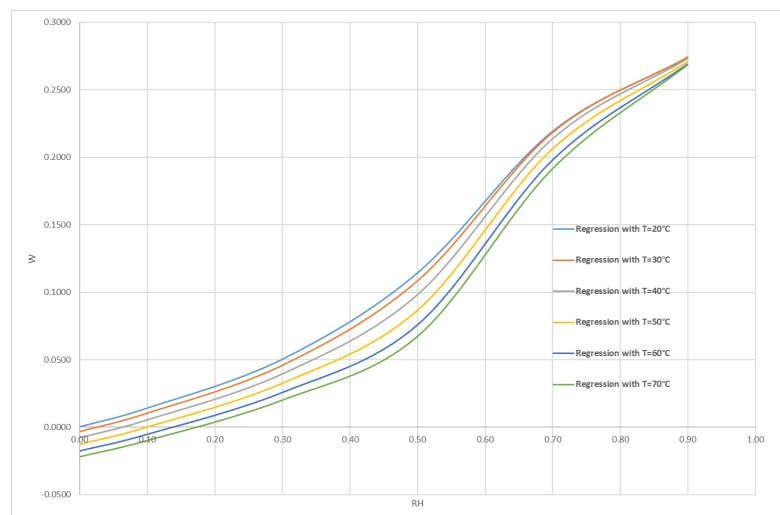


Figure 4.5: Regression of family isotherm curves from 20°C to 70°C.

4.2 Silica gel simulation

The prototype assembled in the laboratory of the Energy Department was already tested mainly with an adsorption heat exchanger that use as sorbent silica gel grains loose inside the fins.

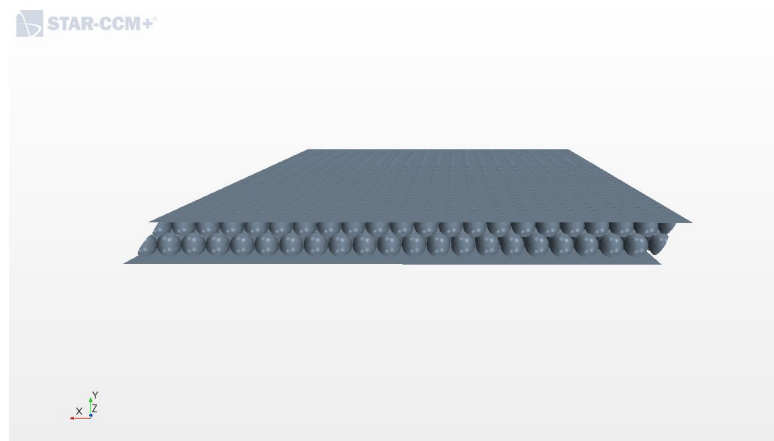


Figure 4.6: Simulation domain with a periodic condition repeated 20 times.

For this reason, the CFD simulations with the software STAR-CCM+ were done firstly with this configuration, in order to compare CFD results with experimental data. First of all the geometry of the system was developed, according to the dimensions of the component. The HX-ADS is $60 \times 60 \times 10 \text{ cm}$ where the air has an inlet surface of $60 \times 60 \text{ cm}$ and pass through the spheres for 10 cm . The space between the fins is 5 mm and the average diameter of the sphere is 3 mm . According to these specifications, the domain of the simulations is the volume between to fins, full of silica gel spheres.

The distribution of the spheres inside the volume shall be such as to obtain the same solid volume ratio of the experimental device. Moreover, to reduce the computational cost of the simulations a periodic condition was imposed for the lateral direction of the fin. In this way only a row of sphere is simulated, so the time of the simulations is greatly reduced but, on the other hand, the effects of the edge condition are neglected. The simulation geometry with a periodic transformation repeated 20 times is shown in Figure [4.6](#).

The software allows to model a fluid flow inside a solid region only using a porous media region, but this increase the computational time of the simulation. To avoid this issue the silica gel spheres has been modelled as a void region in which all adsorption effects are located on the surface of the grains.

The system can be defined as Gas Side Model.

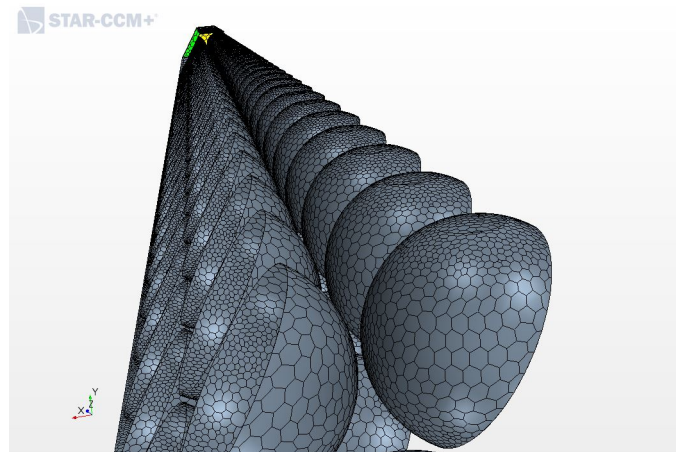


Figure 4.7: Volume mesh

Then, once done the geometry of the system, the following step is to build the mesh. In this specific case, a the mesh was built with the following models:

- Surface Remesher
- Automatic Surface Repair
- Polyhedral Mesher
- Thin Mesher
- Prism Layer Mesher

The base size of the mesh was set equal to $0.001m$.

Moreover, in order to fully develop the fluid flow the domain was extended using two volume extruder, one for the inlet and one for the outlet.

As a matter of fact, using orthogonal extrusions permit to have enough distance for the full development with a low cell count.

The extrusion distance is $5cm$ along a direction normal to the inlet and outlet surface. Then the two extrusions were divided into 24 layers each, using a stretching function that converges towards the surface of the original domain, so one to the inlet and one to the outlet.

A detail of the outlet extruder is shown in Figure [4.8](#).

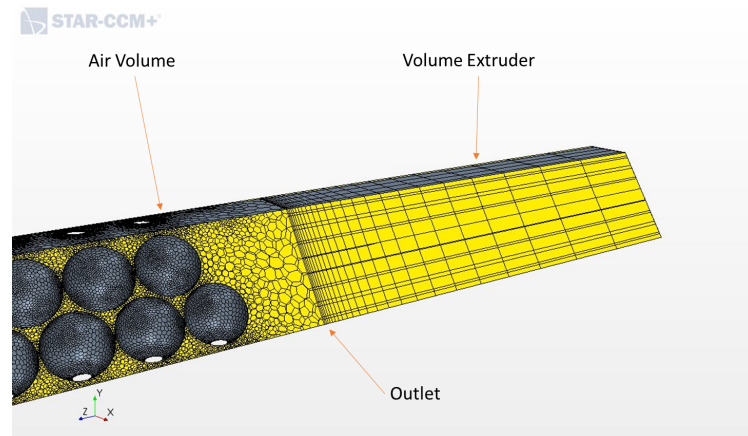


Figure 4.8: Outlet volume extruder

After the definition of the geometry and the creation of the mesh, the following step is to define the physic models used by the software to solve the simulation. In this particular case of silica gel spheres, the system is made only by the air that pass through the adsorbent.

Thus modelling only one substance, must be defined only one physics continuum. A physic continuum contain a set of models for a single region. In this simulation the model used are:

- Three Dimensional
- Implicit Unsteady: Each time step a certain number of inner iterations are solved in order to make converge the solution.
- Multi-component Gas: It is used to model a gas mixture made of two or more components. In this case this model is used to simulate a mixture of air and water vapour.
- Non-reacting
- Ideal gas: This model uses the ideal gas law in order to calculate the density as a function of temperature and pressure.
- Segregated Flow: It used the segregated solver which computes each of the momentum equations in turn, one for each dimension.

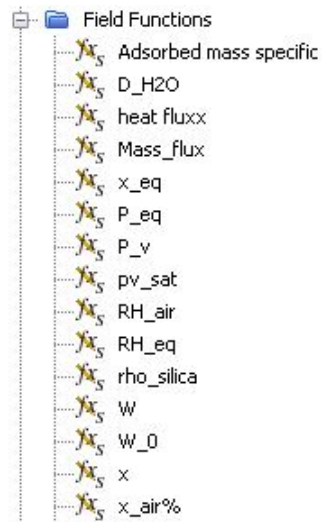


Figure 4.9: *User-defined Field function* used in STAR-CCM+ to implement the theoretical model.

- Gradients: It permits to specify the gradient method, that in this case is Hybrid Gauss-LSQ.
- Segregated Fluid Temperature: This model solves the total energy equation using the temperature as the solved variable. Then the enthalpy is computed starting from the temperature using the equation of state.
- Segregated Species: It is used to solve the species continuity equations for a multi-component gas mixture.
- Laminar

In this simulation the fluid flow through the particles of silica gel is simplified as laminar due to a low velocity of the air at the inlet.

Once done the physics continuum, a region and the boundaries are created. Then, before defining the boundary conditions, the theoretical model of equations used to simulate the adsorption phenomena must be implemented in STAR-CCM+. To do that, a series of *User-defined Field functions* were added, as shown in Figure

[4.9](#)

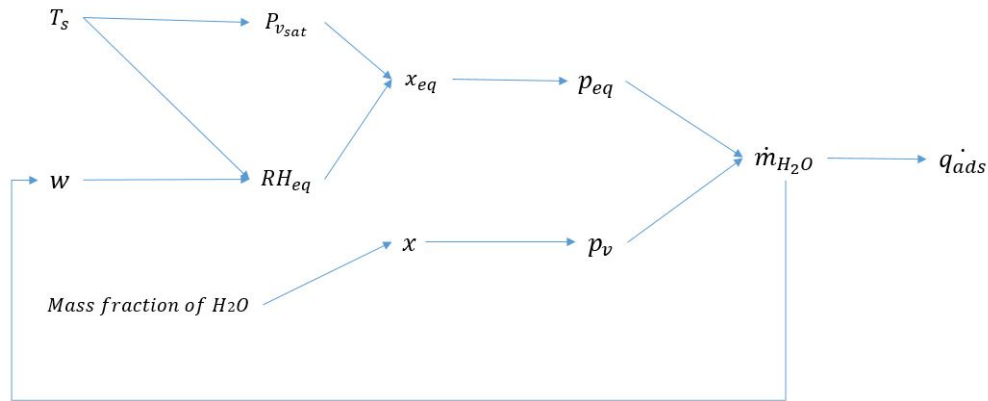


Figure 4.10: Scheme of the variables that the software computes each iteration in order to evaluate the heat and mass flux for each cell.

The *Field functions*, are used to insert in the simulation the set of equations presented in the section [4.1](#). In addition, they are used also to define a series of constants that are involved in the theoretical model, such as the apparent water diffusivity inside the silica gel pores (D_{H_2O}), the density of the silica gel (ρ_{sil}) and the initial water uptake (W_0).

These equations are solved for each cell, and for each iteration starting from the temperature on the surface of the grains and the mass fraction of water in the gas mixture. In addition, the model used also the water uptake (W) as input variable, but it is calculated each time step as the sum of the adsorbed specific mass in the previous time steps, per unit of mass of the desiccant. A scheme of the model of equations is presented in [Figure 4.10](#).

Subsequently, once the field functions are defined, the boundary condition must be set. The geometry of the domain required six boundaries conditions that are shown in [Figure 4.11](#).

At the inlet boundary a *velocity inlet* condition is set. This boundary type is typically used at the inlet of a duct and permits to specify the velocity of the flow. The outlet was set as *flow-split outlet* with a split ration equal to 1. In fact all the gas flow exits through the outlet. As a matter of fact, in the domain there is only

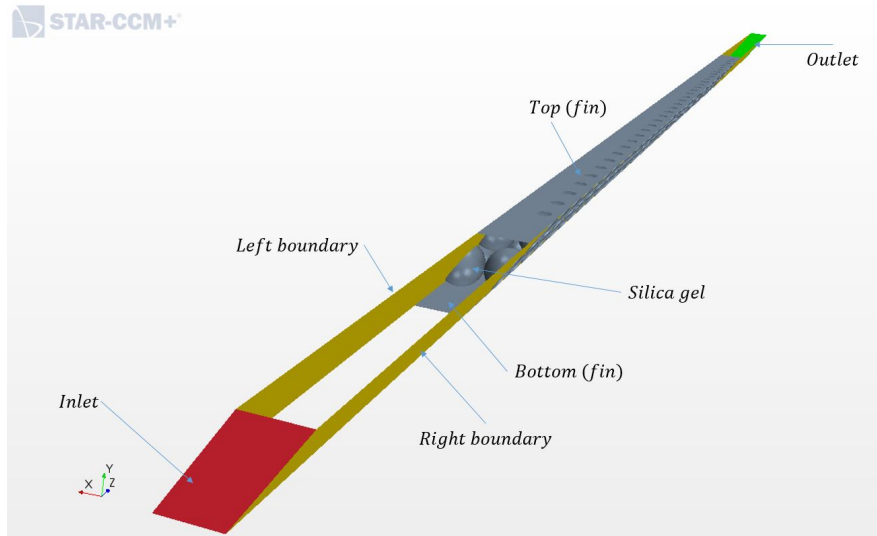


Figure 4.11: Boundaries of the simulation domain.

one outlet. The right and the left boundaries are combined to create a *periodic interface*. In this way is possible to simulate only one row of sphere reducing a lot the computational time.

Then the top and bottom boundaries represent the fin that is considered at a constant temperature, equal to the recirculating temperature of the water that flows into the pipes. Hence the *Thermal specification* is set to *Temperature* and then the static temperature can be imposed.

Finally the silica gel boundary is used to simulate the heat and mass flux related to the adsorption phenomenon. To do that the *Thermal specification* is set to *Heat flux* and the *Method* to *Field function*. Then the adsorption heat flux field function must be selected.

According to these specification the software evaluates the \dot{q}_{ads} for each cell of the boundary. In addition, the mass flux related to the adsorption must be imposed on the silica gel boundary. The *Wall Species Option* is set to *Specified Flux*. Then, in order to consider separately the mass flux of water and air the *Method* selected is *Composite*.

Now the air flux through the silica gel is imposed constant and equal to $0 [kg/m^2s]$, while the water mass flux is inserted as a *Field function*.

In this node the adsorption mass flux is selected.

Now, the pre-processing is defined, so the following step is to define the solvers and the stopping criteria. In this case, the software solved a transient so the stopping criteria are related to each time step, in order to reach the convergence before starting the following time step. The time-step of the simulation was imposed to 30s as a good compromise between results and computational cost. The stopping criteria for each inner iterations are:

- Air Criterion
- H_2O Criterion
- Continuity Criterion
- Energy Criterion
- X-momentum Criterion
- Y-momentum Criterion
- Z-momentum Criterion

All of these stopping criteria must be valid at the same time, and each one must be lower than 1.0E-4.

In addition, a maximum value of inner iterations is imposed if the stopping criteria do not reach the convergence in a certain number of iterations. In this case 1000 inner iterations were selected as the maximum limits but typically the simulation converges with a lower value. A plot of the residuals of the simulation is shown in Figure [4.12](#).

Finally a maximum physical time can be set in order to stop the simulation when the transient terminates. A value of 6000s was imposed to the adsorption phase and then 12000s, to simulate the regeneration of the adsorbent material. The last part of the simulation in a CFD software is the post-processing. In this case a series of reports, plots and scenes were created in order to monitor the simulation results during the transient. In particular reports and plots are used to monitor:

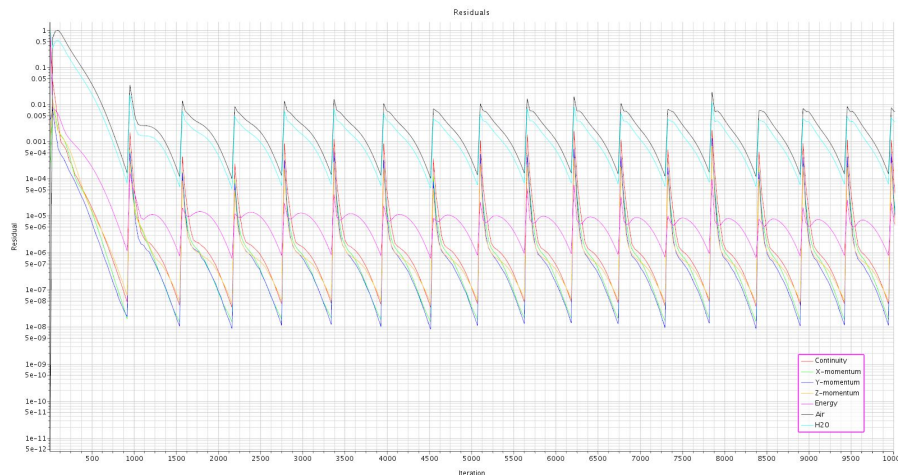


Figure 4.12: Residuals of the simulations during the first 17 time-steps.

- Mass adsorbed of water
- Mass flux
- Pressure drop between the inlet and the outlet
- Water uptake(W)
- Relative humidity of the air at the inlet and at the outlet
- Temperature from the inlet to the outlet each $1cm$ as an average value on a surface normal to the fluid flow direction
- Moisture content from the inlet to the outlet each $1cm$ as an average value on a surface normal to the fluid flow direction

The simulation computes an adsorption cycle of $6000s$ with a fin temperature equal to $21^{\circ}C$ and a regeneration cycle of the same time, with a fin temperature of $62.5^{\circ}C$. The following figures shown plots and scenes of the simulation in different time steps.

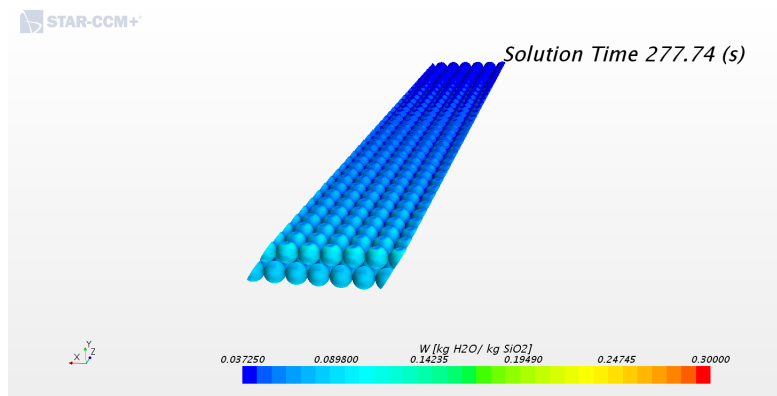


Figure 4.13: Scene of the water uptake after 5 minutes of adsorption.

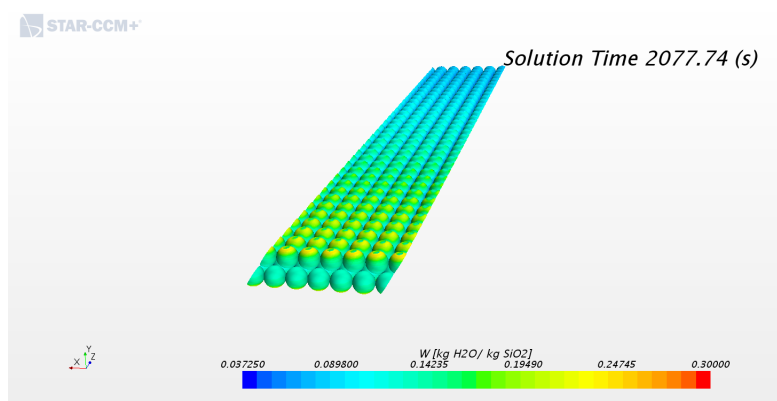


Figure 4.14: Scene of the water uptake after 35 minutes of adsorption.

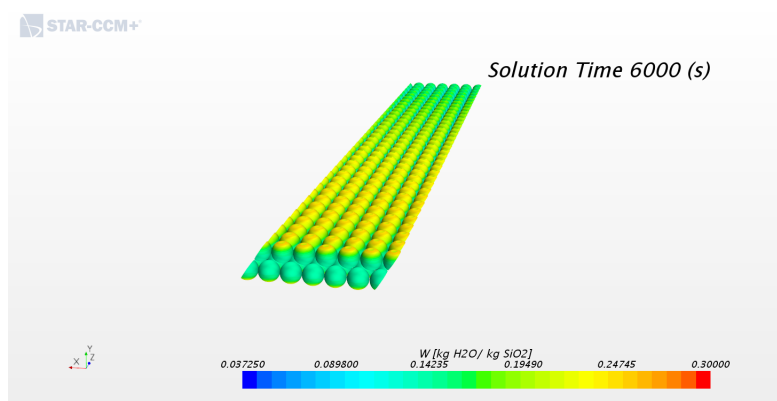


Figure 4.15: Scene of the water uptake at the end of the adsorption cycles(100 minutes).

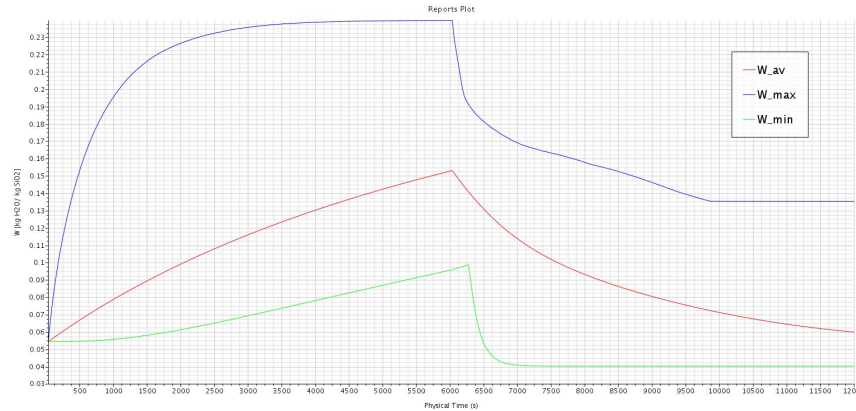


Figure 4.16: Plot of the maximum, minimum and average value of water uptake on the silica gel boundary during the whole transient.

4.2.1 Comparison with experimental test

This work presents a model to simulate, with a CFD software, the adsorption phenomena inside an adsorption heat exchanger in order to study different configurations, changing parameters such as the geometry or the materials. First of all, it is necessary to compare a simulation with an experimental test done in the laboratory in order to validate the model from the adsorption point of view. The main properties that have to be compared are the temperature profile, the moisture content, the adsorbed mass and the pressure drop. In the laboratory, some prototypes were tested.

The calibration of the model was carried out with a test done in the July 2018, using an HX-ADS with silica gel grains. In more detail, the system worked for more than 7 hours computing in series, adsorption and desorption cycles. Using sensors assembled on the prototype, several data were collected. In particular, the main quantities monitored are:

- Temperature of the cold water of the recirculating system
- Temperature of the hot water of the recirculating system
- Inlet temperature of the air

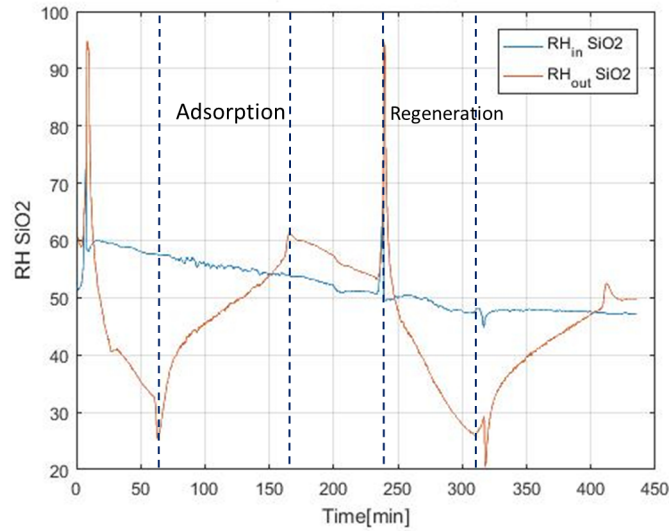


Figure 4.17: Transient of the inlet and outlet relative humidity of the air during the test.

- Outlet temperature of the air
- Inlet relative humidity of the air
- Outlet relative humidity of the air

The transient of these quantities during the whole test are shown in Figures [4.17](#), [4.18](#), [4.19](#), [4.20](#).

Then, starting from these data, the air moisture content was calculated as:

$$x = 0.622 \cdot \frac{RH \cdot p_{v_{sat}}}{p_a - RH \cdot p_{v_{sat}}} \quad (4.11)$$

Results are shown in Figure [4.21](#).

In order to valid the CFD model of the adsorption heat exchanger, a cycle of adsorption and one of regeneration were chosen as comparison. In particular, the adsorption cycle starts at the minute 62 and terminates at 162, so the duration of the cycle is 100 minutes. Instead the regeneration cycle starts at the minute

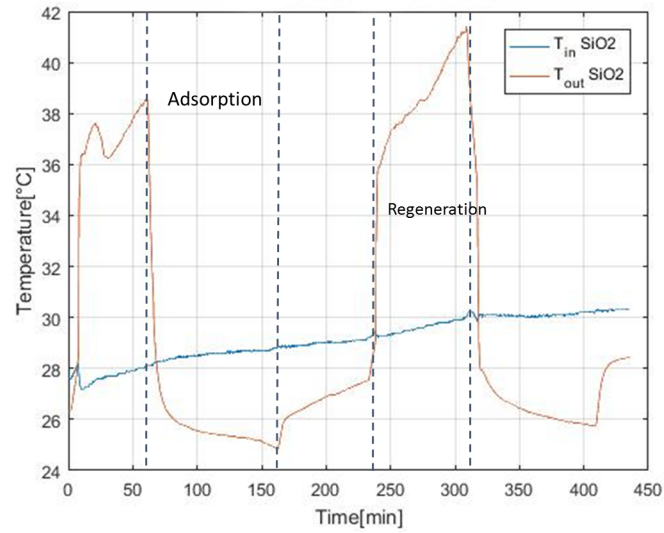


Figure 4.18: Transient of the inlet and outlet temperature of the air during the test.

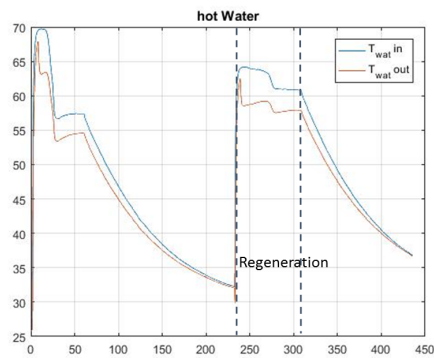


Figure 4.19: Temperature of the hot water recirculating system during the test.

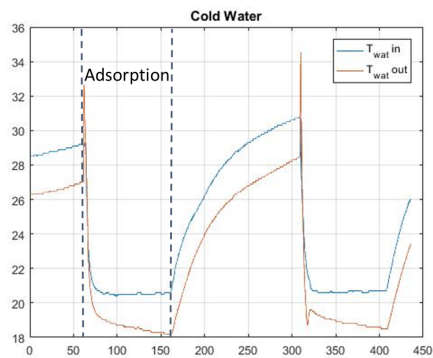


Figure 4.20: Temperature of the cold water recirculating system during the test.

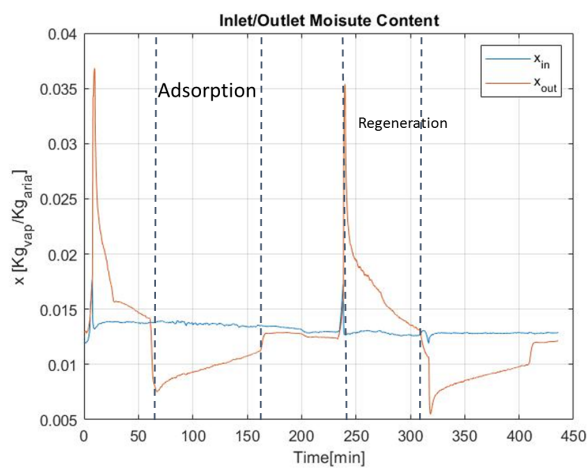


Figure 4.21: Transient of the inlet and outlet air moisture content of the air during the test.

Table 4.2

ADSORPTION			REGENERATION		
time	100	[min]	time	70	[min]
v_{in}	0.25	[m/s]	v_{in}	0.25	[m/s]
HR_{in}	54.3	[%]	HR_{in}	49.6	[%]
T_{air-in}	27.5	[°C]	T_{air-in}	28.5	[°C]
$T_{hot-water}$	21	[°C]	$T_{cold-water}$	62.5	[°C]

240 and finishes at the minute 310 so, in this case, the duration of the desorption is 70 minutes.

The input variables, as visible in the charts, present a small variation during the transient. These operating conditions is simplified as constant in the simulation, equal to a mean value of the variation range. The operating condition of the test, used as input variables in the CFD simulation, are reported in table 4.2.

The simulation was used to simulate the same transient, simulating in series an adsorption cycle of 100 minutes and a following regeneration cycle of 70 minutes. In particular, the comparison of the CFD results with the experimental data was performed using the temperature of the air, the relative humidity and the air moisture content at the inlet and at the outlet. The air moisture content is a function of the temperature and the relative humidity so if these two quantities are valid in the CFD model also the third one is valid. On the contrary looking at the air moisture content if there are variations between CFD results and experimental data they can be caused by the temperature profile or by the relative humidity profile. The transients of the temperature and the relative humidity at the outlet during both adsorption and regeneration cycles are shown in Figures [4.22](#), [4.23](#), [4.24](#), [4.25](#).

The main issue regarding the transients described by the CFD model is evident in the temperature charts. In fact, both in adsorption and desorption, the temperature profile obtained with the software does not have the same behaviour of the outlet temperature measured on the prototype. This problem occurs because simulating the system in such a way, the simulation does not perform the solid

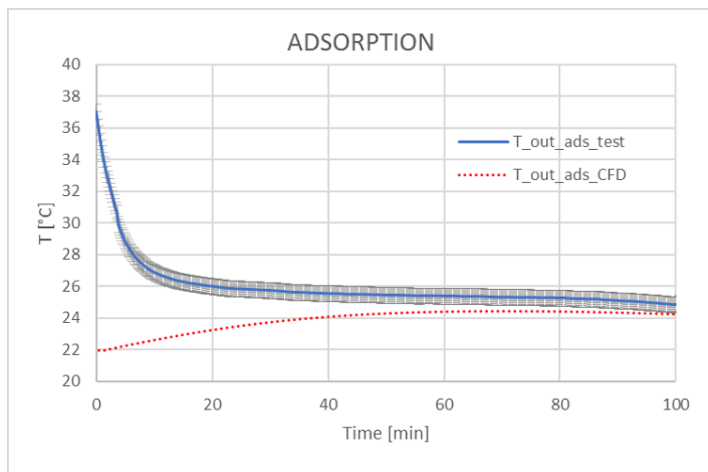


Figure 4.22: Comparison between experimental data and CFD results.

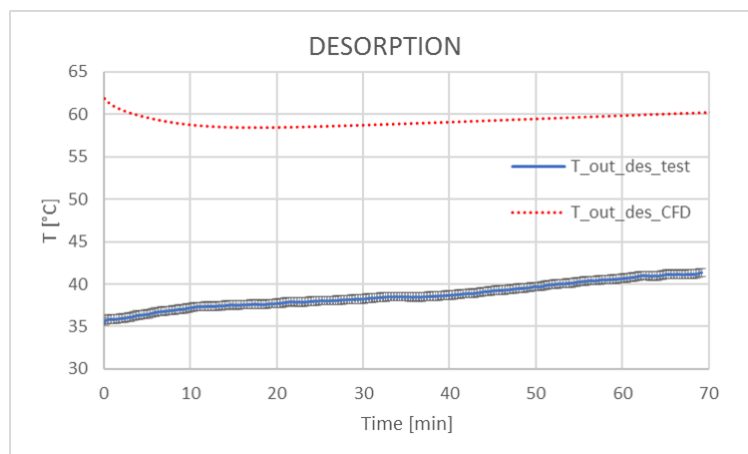


Figure 4.23: Comparison between experimental data and CFD results

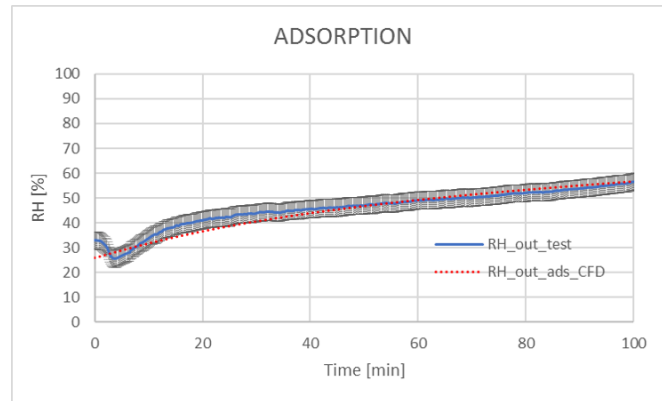


Figure 4.24: Comparison between experimental data and CFD results

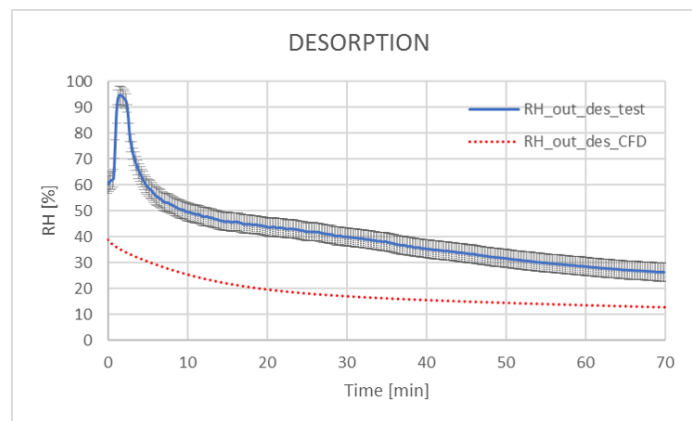


Figure 4.25: Comparison between experimental data and CFD results

region of the adsorbent, so its thermal inertia is not calculated.

For instance, in Figure 4.22, during the adsorption real transient the outlet temperature decreases while in the results of the simulation it increases. The decreasing trend is related to the fact that initially the silica gel spheres are at high temperature ($\sim 60^{\circ}\text{C}$) due to the previous regeneration cycle and then during the adsorption the temperature decreases thanks to the recirculating water. In addition, another problem with respect to the temperature profile, is observable in Figure 4.23. As a matter of fact, mainly during the regeneration cycle, it is clear that the approximation of the fin profile with a constant temperature, equal to the recirculation water temperature, is not correct because the outlet temperature evaluated by the software is higher compared to the experimental data.

Then, in order to avoid these issues, some changes in the model are required. In particular, it is necessary to implement inside the model the evaluation of the temperature of the spheres considering their thermal inertia. In that way is possible to compute also the convection heat transfer between the air and the adsorbent material. In conclusion, the model needs to simulate also the transient of the temperature of the silica gel surface and it requires also a different temperature boundary condition on the top and bottom boundaries.

4.2.2 Simulation with the temperature of the spheres

In the previous paragraph, a comparison with experimental data was performed. The CFD results present a different behaviour compared to the test, mainly from the temperature point of view. As a matter of fact, the temperature profiles, both in adsorption and in the regeneration, highlight that the thermal inertia of the silica gel spheres must be considered in order to have in the simulation, the same profile measured in the test.

To do that, the transient of the temperature on the surface of the grains must be implemented. To evaluate the evolution of the temperature of the grains is necessary to consider the variation of heat adsorbed by the spheres. In this specific case, starting from the data calculated by the software the variation of the heat of the grains was calculated as:

$$\Delta Q = \frac{\rho_{sil} \cdot V_{cell} \cdot cp_{sil} \cdot (T_{sil} - T_{air})}{\Delta t \cdot Area_{cell}} \quad \left[\frac{W}{m^2} \right] \quad (4.12)$$

Then, in order to calculate the transient of the T_{sil} during the whole simulation a *monitor* was used. In particular, starting from an initial value (T_0), the *monitor* evaluates for each time step the variation (ΔT_{sil}) respect to the previous one.

ΔT_{sil} is evaluate as:

$$\Delta T_{sil} = \frac{(\dot{q}_{ads} - \Delta Q) \cdot \Delta t \cdot Area_{cell}}{\rho_{sil} \cdot V_{cell} \cdot cp_{sil}} \quad [K] \quad (4.13)$$

Each time step, the monitor updates the temperature of the silica gel spheres thanks to the variation of heat exchanged. Finally the heat flux on the surface of the grains is set equal to the sum of the adsorption term and ΔQ .

In addition, also the temperature boundary condition on the top and bottom boundaries was changed. Analysing the transient of temperature during regeneration is visible that the final value that it reaches is 42°C. Considering that the air enters in the system at very low temperature can be deduced that the temperature of the fins is similar to this value. For this reason a temperature of 42°C was used as condition fro the top and bottom boundaries during desorption. For the same reason, during the adsorption, the temperature condition was set equal to 23°C instead of 21°C.

The temperature profiles obtained in the new simulation, compared to the experimental data, are shown in Figures [4.26](#) and [4.27](#).

In this case, they present the same behaviour of the transient measured during the test. In the regeneration is more clear that profile has a more stationary behaviour compared to the test, because the fin is simulated with a constant temperature during time, while in the reality it changes due to the recirculating water. To obtain more precise results from the temperature point of view also the solid fin can be modelled but with an increment of computational time. In such a

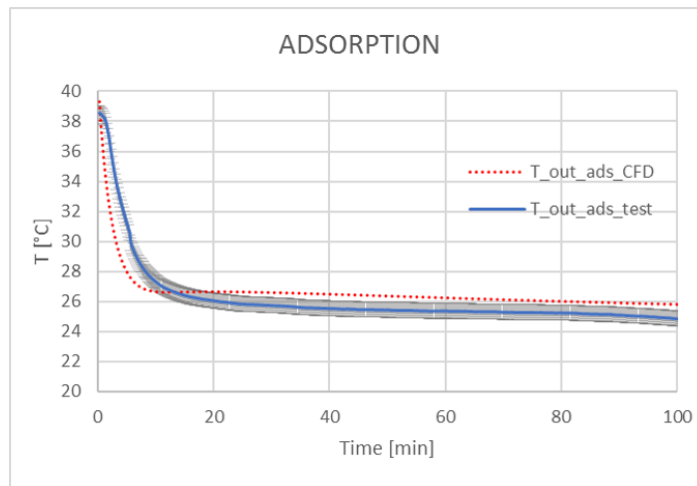


Figure 4.26: Comparison between experimental data and CFD results.

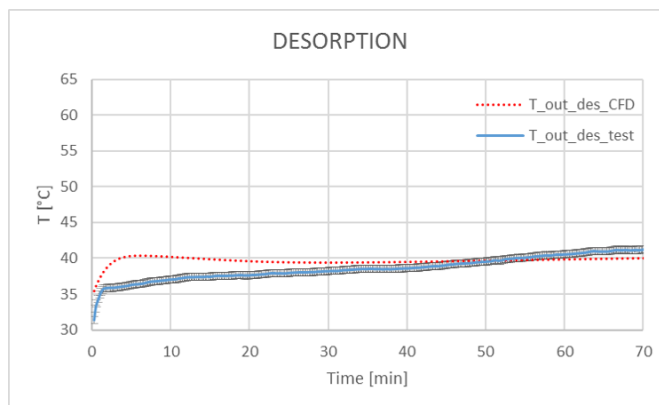


Figure 4.27: Comparison between experimental data and CFD results.

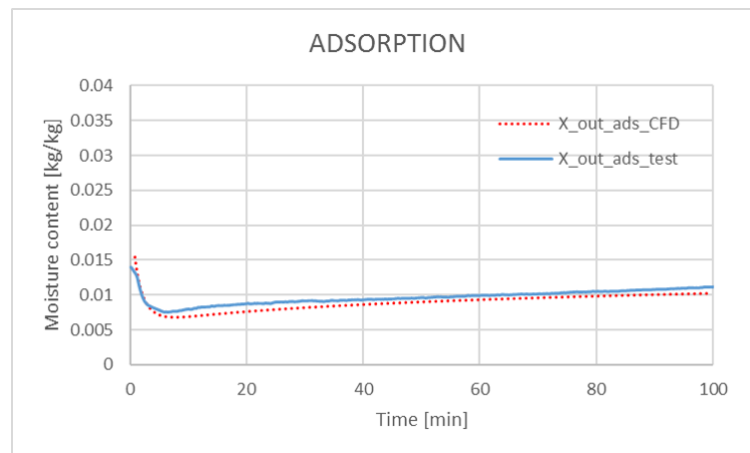


Figure 4.28: Comparison between experimental data and CFD results.

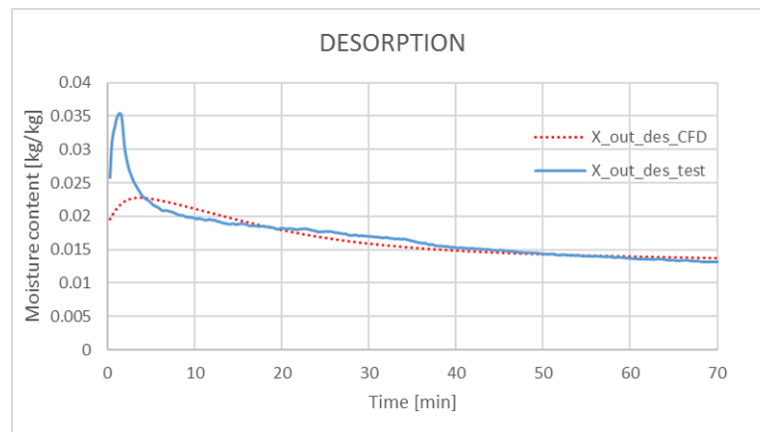


Figure 4.29: Comparison between experimental data and CFD results.

way, the temperature profile reaches a good compromise between computational time and precision. Indeed it permits to evaluate with an high precision also the air moisture content, validating the model from the mass exchange point of view. This can be seen in Figures [4.28](#) and [4.29](#), where the air moisture content calculated with the CFD simulation is compared to the experimental data.

The absolute and relative errors between the air moisture content obtained in the test and the value evaluated with the simulation, expressed in grams of water per kilograms of dry air are shown in Figures [4.30](#) and [4.31](#).

During the whole simulation the error is lower than the 1 $[g_{water}/kg_{air}]$, except

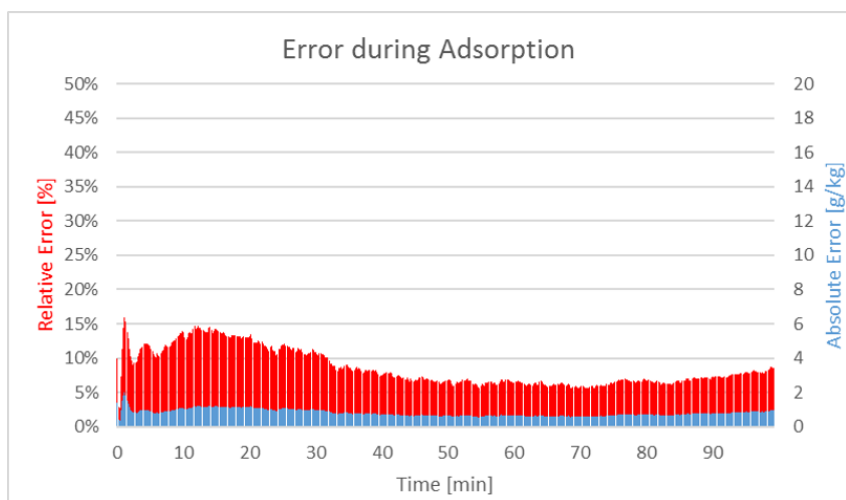


Figure 4.30: Comparison between experimental data and CFD results.

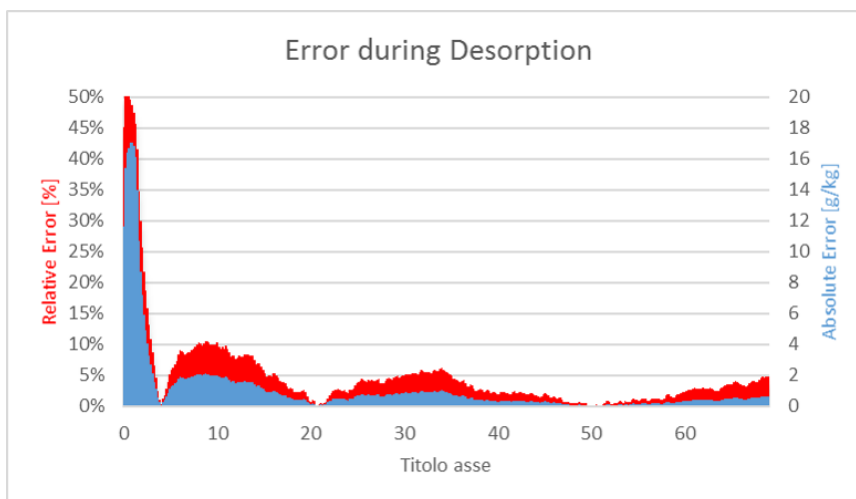


Figure 4.31: Comparison between experimental data and CFD results.

for the initial transient of the regeneration. This is mainly related to the temperature profile that changes rapidly compared to the real one due to the absence of the solid fin.

In conclusion, the HX-ADS can be simulated also neglecting the solid region of the fin. This allows a reduction of the computation time while still assuring a high degree of accuracy in the air moisture content evaluation.

Chapter 5

Extension of the model for a coated HX-ADS

As seen in the previous chapters, different configurations can be adopted for adsorption heat exchanger. In particular the most used are a finned heat exchanger loaded with grains of adsorption materials or a coated finned heat exchanger. The simulation used to valid the model was performed modelling a HX-ADS loaded with silica gel grains so in order to use the same model for a coated configurations an extension of the model must be done.

In particular the main difference between the two configuration is that in the first case the adsorption phenomena are simulated on the sorbent surface and the temperature of the fin is imposed on a boundary of the air. In a coated configuration, without modelling the coating, the two boundary conditions must be set in the same surface.

The software does not allow to impose both an heat flux and a temperature profile on the same boundary. For this reason an alternative way to simulate the coating has to be used.

A possible solution can be the simulation the coating as a solid region imposing the adsorption heat flux on the internal surface, the one in contact with the air, and the fin temperature profile on the external surface.

Also in this case there are problems with the software because in the internal

interface, between the air and the coating, a mass flux cannot be imposed. As a matter of fact, simulating the system in this way, a water mass flux enters in the solid region and this is not allowed by the software.

To avoid this issue a different solution can be adopted. Indeed, the regions can be split in two different bodies without interfaces. Then, the two regions must be coupled in order to solve the temperature profile and the heat flux on the surface of the air in contact with the coating. In this way is possible to simulate also the temperature profile of the fin crossed by the recirculating pipes.

To do that an additional hypothesis must be done:

- The temperature profile on the interface between the coating and the fin is equal to the temperature profile on the interface between the coating and the air. It means that the thermal resistance of the coating is neglected.

This assumption can be done mainly because the thickness of a coating is typically very low, thinner than $1mm$.

For instance, considering a coating with a thickness(t_c) of $1mm$ and a generic zeolite thermal conductivity(k) from literature^{[37][38]} equal to $0,32 [W/mK]$, the thermal resistance is of the order of 10 to the minus 3.

$$R = \frac{t_c}{k} = \frac{10^{-3}}{0.36} = 2.7 \cdot 10^{-3} \quad [K/W] \quad (5.1)$$

Simulating a finned HX-ADS with this methodology permits to consider the temperature profile of the fin that changes during the transient, affected both by the recirculating water and the adsorption heat generation.

The adsorbed mass of water, such as in the silica gel simulation, is considered monitoring along the transient the sum of the mass flux integrated over time, on the whole coating surface.

In addition, another advantage compared to the silica gel model, is that the simulation of the fin, with its temperature profile, permits to consider the thermal inertial term related to the fin, permitting to test different configurations with different materials and thickness.

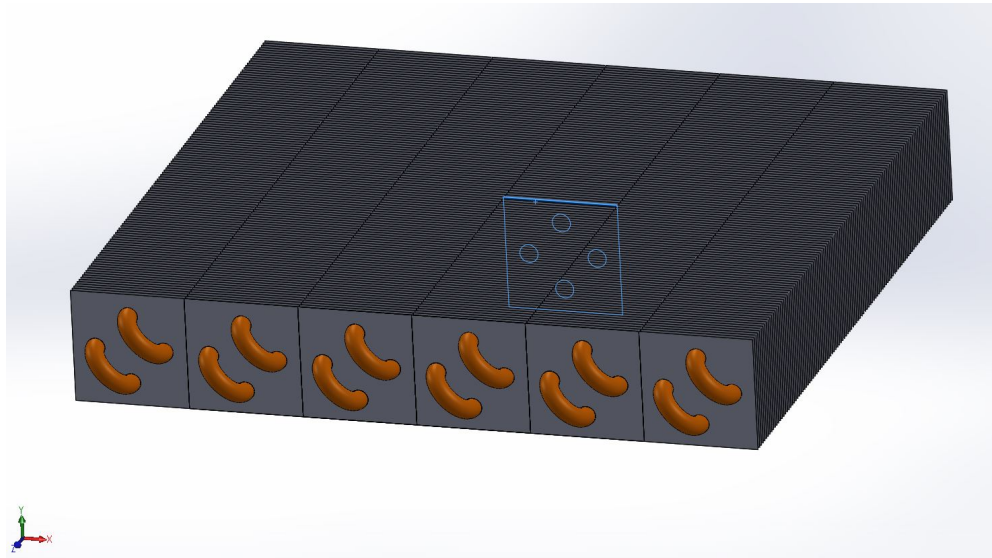


Figure 5.1: finned HX-ADS design. The geometry of the simulation is highlighted.

5.1 Simulation of an adsorbent coating in a finned heat exchanger

In this section a simulation of an adsorption coating on a fin is presented. The difference compared to a normal coating is that a mass flux of water occurs over the interface between the air and the coating. In order to simulate this phenomenon the simulation solved separately the air region and the fin, coupling them with surface *Data Mapper*.

The geometry was built accordingly to adsorption heat exchanger used in the prototype tested in the laboratory. In particular, in order to take advantage of the symmetry, to reduce the computational cost, only a small part of the component was simulated.

A view of the design of the adsorption heat exchanger is presented in Figure [5.1](#).

In more detail, the simulation domain is made of a central part of the component with dimension $100 \times 100 \times 2,6 \text{ mm}$. The thickness is the sum of the air region and the fin, that are respectively $2,5 \text{ mm}$ and $0,1 \text{ mm}$. In the real component the distance between two fins is 5 mm and the thickness of a fin is $0,2 \text{ mm}$ but also in

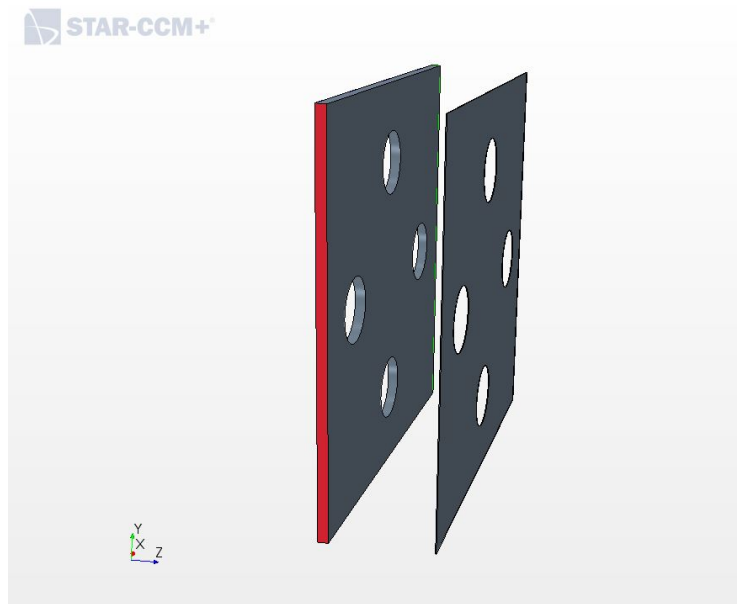


Figure 5.2: Simulation geometry.

this case the symmetry was considered. As mentioned before, the air region and the fin are decoupled. The distance between the two bodies is arbitrary and does not represent the thickness of the coating.

t_c is considered in a *Field function*, as explained subsequently. Finally the domain of the CFD simulation is presented in Figure 5.2.

Then the following step is to define the mesh. In this case two different meshes were generated for the two regions, one for the air and one for the fin. The models used for generating the meshes are the same:

- Surface Remesher
- Automatic Surface Repair
- Polyhedral Mesher
- Prism Layer Mesher

The base size of the mesh was set equal to $0.005m$ for the fin and $0.001m$ for the air. Then in order to obtain two equal meshes on the surfaces that will be

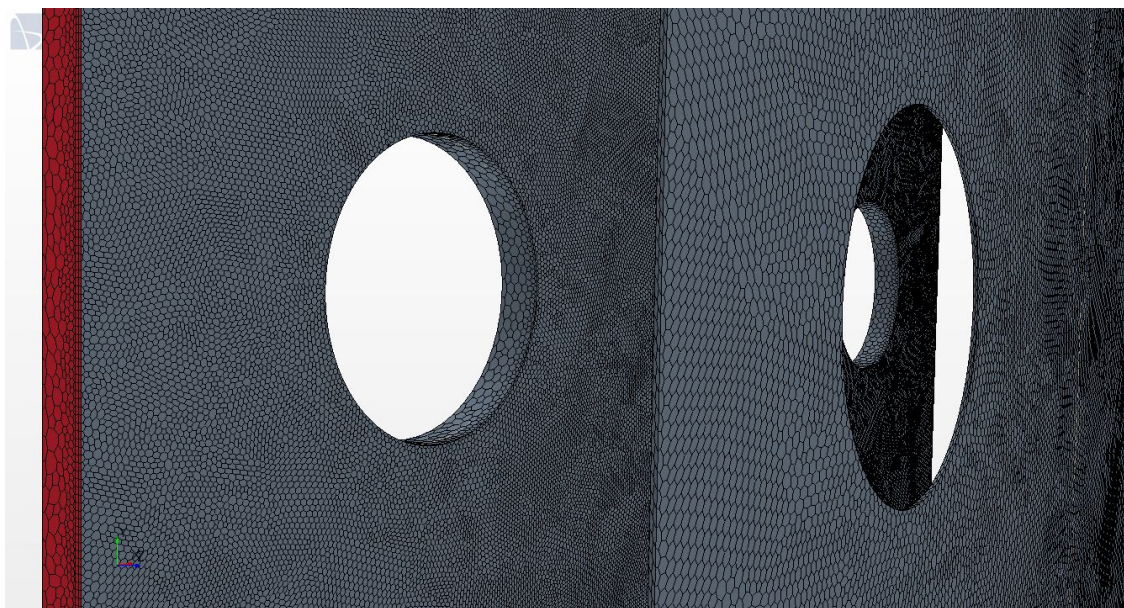


Figure 5.3: Meshes of the two regions of the simulation domain.

coupled, two different *Surface control* were used.

This function permits to generate a mesh of a different size on a particular surface. Hence, a *Surface control* was used in the mesh of the air, applied on the surface "in contact" with the fin, to produce a denser mesh. Equally, in the fin region a *Surface control* was set to generate a mesh with the same base size of the air. In these two surfaces the base size were imposed equal to $3E-4m$. The resulting mesh is shown in Figure [5.3](#).

Then, the following step is to set the physics continua of the regions.

In this case, differently from the silica gel simulation, there are two regions, one for the air and one for the fin. Therefore, the model requires two physics continua. As in the previous example, the models selected for the air are:

- Three Dimensional
- Implicit Unsteady
- Multi-component Gas
- Non-reacting

- Ideal gas
- Segregated Flow
- Gradients
- Segregated Fluid Temperature
- Segregated Species
- Laminar

The laminar model was set according to the physics of the phenomenon. As a matter of fact, in case of fluid flow between parallel plates the flow can be consider laminar when the Reynolds number is lower than 1400. In this case it results:

$$Re = \frac{\rho_{air} \cdot v_{in} \cdot D_H}{\mu_{air}} = \frac{1.225 \cdot 0.25 \cdot 0.01}{1.81 \cdot 10^{-5}} = 169.2 \quad (5.2)$$

Where ρ_{air} is [kg/m^3], v_{in} in [m/s], μ_{air} is the dynamic viscosity of the air and it is in [$Pa \cdot s$]. D_H is the hydraulic diameter [m] that in case of parallel plates can be consider equal to $2D$, where D is the distance between the plates. In this specific simulation the distance between the fins in $5mm$. For the solid region that represents the fin, different physics models were selected:

- Three Dimensional
- Implicit Unsteady
- Solid
- Constant Density
- Segregated Solid Energy
- Gradients

After the definition of the physics continua, and their coupling with the regions, the *Field functions* that describe the adsorption phenomenon must be added. The *User-defined Filed functions* are the same of the previous simulation, illustrated in Figures [4.9](#) and [4.10](#). The property of the material, such as ρ , D_{H_2O} and RH_{eq} , must be changed according to the material that has to be modelled.

In addition, the main difference compared to the simulation with adsorbent spheres is the definition of the water uptake(W). As seen in the formula the water uptake depends on the mass of the adsorption material that can be collect water.

In this case V_c is:

$$V_c = Area_{cell} \cdot t_c \quad (5.3)$$

Therefore, to define the thickness of the coating, it must be considered in the water uptake *User-defined Field function*.

The following step is to define the boundary conditions, but in this a case is necessary to define two *Data Mappers* first. The *Data Mapper* is a tool of STAR-CCM+ that allows to interpolate field data available either on a surface mesh or on a volume mesh, so that the mapped fields can be used for applying boundary or volume conditions on the target mesh [39](#). In this case it is used to coupled the air region with the fin and vice versa. The two *Data Mappers* defined for this simulation are:

- Heat flux: It is a surface to surface *Data Mapper* that maps the adsorption heat flux profile at the external air surface and then it used to define the boundary condition of the internal surface of the fin.
- Temperature: It is a surface to surface *Data Mapper* that maps the temperature profile at the internal fin surface and then it used to define the boundary condition of the external surface of the air.

These tools permit to coupled the heat transfer between the gas and the solid region.

The boundary of the simulation domain are shown in Figure [5.4](#).

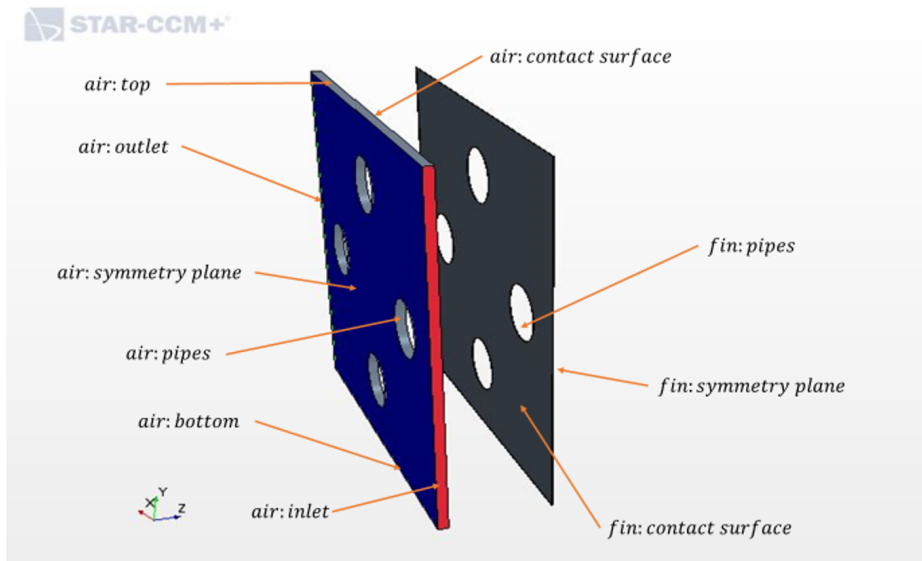


Figure 5.4: Boundaries of the simulation domain.

They were set as follow:

- Air:
 - Inlet: *velocity inlet*;
 - Outlet: *flow split outlet*. With split ration equal to 1.
 - Symmetry plane: *symmetry plane*.
 - Contact surface: *Thermal specification* equal to *Temperature*. Then the *Field Function* has been used as *Method*, and finally the *Temperature Data Mapper* has been recalled. In addition, the water mass flux is imposed as *Field function*.
 - Pipes: *Thermal specification* equal to *Temperature*. A constant temperature can be imposed.
 - Top and Bottom: a *periodic interface* has been imposed according to the geometry of the whole component.
- Fin:

- Symmetry plane: *symmetry plane*.
- Contact surface: *Thermal specification* equal to *Heat Flux*. Then the *Field Function* has been used as *Method*, and finally the *Heat Flux Data Mapper* has been recalled.
- Pipes: *Thermal specification* equal to *Temperature*. A constant temperature can be imposed.
- Top and Bottom: a *periodic interface* has been imposed according to the geometry of the whole component.
- A condition of adiabatic wall has been selected for the corresponding inlet and outlet of the fin.

Then, after the pre-processing definition, the solvers must be imposed.

The CFD simulation solved a transient so a time-step has to be selected. In this case the simulation in the first iterations needs a low Δt in order to reach the convergence. For instance, a time-step of 1s can be imposed.

Then, once that the system is more stable, the time-step can be increased up to 30s, reducing the computational time. Like in the previous simulation, the stopping criteria that the software imposes each Δt are:

- Air Criterion
- H_2O Criterion
- Continuity Criterion
- Energy Criterion
- X-momentum Criterion
- Y-momentum Criterion
- Z-momentum Criterion

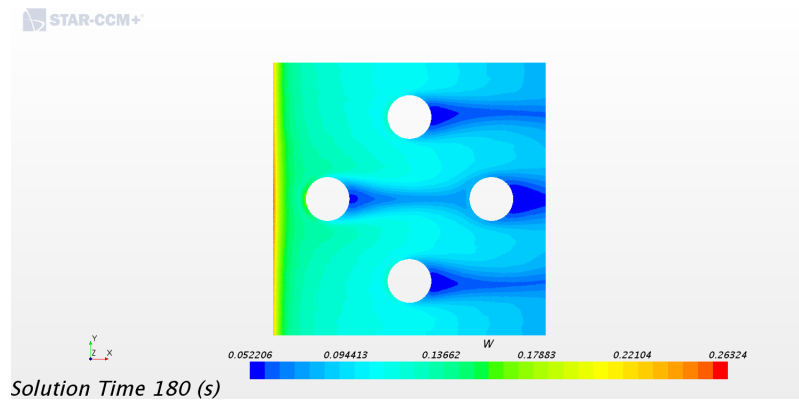


Figure 5.5: Water uptake scene during an adsorption transient.

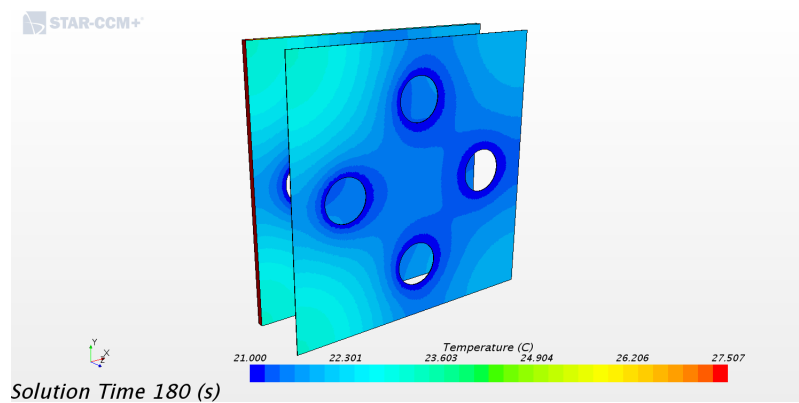


Figure 5.6: Temperature scene during an adsorption transient. The *Temperature Data Mapper* is visible on the two contact surfaces.

Finally, in the post-processing, several data can be collected in order to understand how the system works for different configurations. Scenes that represent the temperature and the water uptake during an adsorption transient are shown in Figures 5.5 and 5.6. Moreover, a transient of the temperature and relative humidity of the air are presented in Figures 5.7 and 5.8.

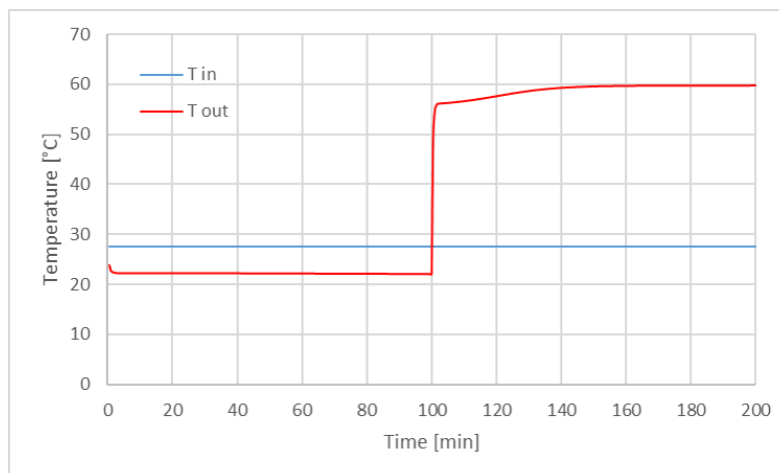


Figure 5.7: Air temperature transient of an adsorption/desorption cycle of 200 minutes. ($t_c = 1mm$)

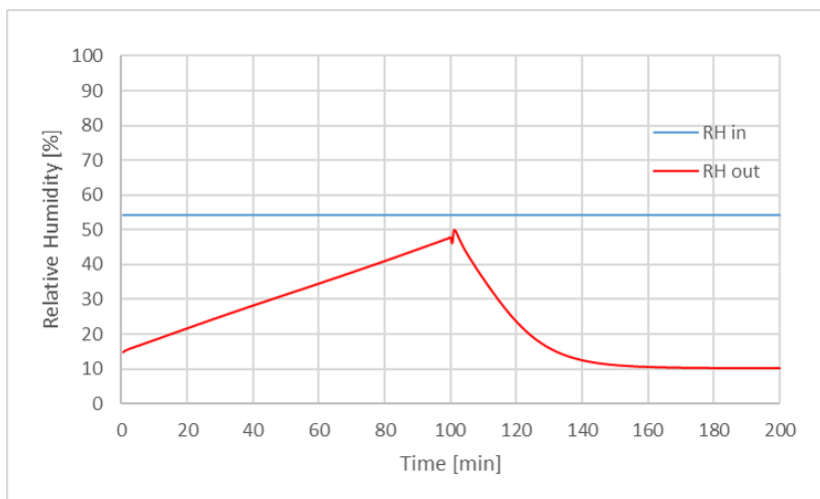


Figure 5.8: Air Relative humidity transient of an adsorption/desorption cycle of 200 minutes. ($t_c = 1mm$)

Chapter 6

Conclusions

In this work is presented a theoretical model of equations implemented in the CFD software STAR-CCM+, used for simulating an adsorption heat exchanger. In particular, the model permits to study the phenomena that occur inside the system such as the heat and mass transfer. The validation of the model has been carried out comparing temperature, relative humidity and moisture content of the air with the experimental data obtained during a test on the prototype assemble in the laboratory of the Energy Department of the Polytechnic of Turin.

In particular, the configuration used for the validation is a finned HX-ADS loaded with silica gel grains. Therefore, the model can be used to studying different configurations. For instance, different geometries and several operating conditions can be simulated to analyse how the system is affected by all these parameters.

The main advantages of the CFD simulations is the strong reduction of time and costs and they allow to have a good estimation of how the system works in different conditions. As a matter of fact, the model are able to estimate the transient of the air moisture content with an absolute error lower than 2 grams of water vapour per kilograms of dry air, as shown in Figures [4.30](#) and [4.31](#).

However, this condition is not verified after rapid variations of the system. For instance, in the transition from adsorption to regeneration and vice versa. In these cases, for a small transient, the absolute error can reaches values up to $14 - 16 [kg_{water}/kg_{dryair}]$. This increasing of the error is mainly because the model

is a simplification of the real case, so some phenomena are neglected. Indeed, in order to reduce the computational time, the solid fin is not simulated so, in the CFD simulation the transient of T and RH are typically faster than in the reality. In addition, the thermal losses due to the heat exchange with the external environment are not considered. Also the thermal mass of the entire set-up is not simulated.

Therefore, due to these simplifications, the model presents faster transient after rapid variation of the operating conditions, such as the temperature of the water in the recirculating pipes. Anyhow, cycles of adsorption and regeneration are typically much longer than the time that the model needs to reduce the error under $1 - 2[kg_{water}/kg_{dryair}]$.

Another issue related to the usage of the model is the determination of the temperature condition at the boundaries that represent the fins. A future work can be the development of a model to determine this temperature as a function of the design and the operating conditions.

The second part of this work presents an extension of the model used to simulate another configuration: a coated finned HX-ADS. In this case, maintaining a relatively low computational time, is possible to simulate also larger domains considering also the solid regions of the fins. For this reason, the part of the error produced by the model due to the absence of the fin is eliminated. In addition, also the issue related to the temperature condition at the boundaries is solved because in this case is possible to set directly the temperature of the recirculating water and the software evaluates also the fin temperature profile.

Finally, for both grains and coating, a future study on the diffusion coefficient of the water inside the adsorption material can be performed. As a matter of fact, D_{H_2O} is strictly linked to the temperature and changes during the transient. In this case it was simplified using a constant value but the error produced by the software during the rapid variation of the operating conditions can be also related to the fact that, in these transients, the diffusion of the water inside the material can be faster or slower compared to the simulated case.

In conclusion, the model can be further improved, reducing the error avoiding an

increasing of the computational time. At the moment, the model can be used to analyse different configurations of adsorption heat exchangers in order to understand how to enhance the performances of the prototype for water harvesting from atmosphere.

Bibliography

- [1] The global challenge: preserving a global resource. Impact series 02. Barclays, Columbia Water Center; 2017.
- [2] Eric Hand. Western U.S. states using up ground water at an alarming rate. Science; 2014. [<http://www.sciencemag.org/news/2014/07/western-us-states-using-ground-water-alarming-rate>]
- [3] <http://mead.uslakes.info/level.asp>
- [4] Amy Maxmen. Cape Town scientists prepare for 'Day Zero'. Nature; 2018. [<https://www.nature.com/articles/d41586-018-01134-x>]
- [5] D. Vanhama, S. del Pozo, A.G. Pekcanc, L. Keinan-Boker, A. Trichopoulou, B.M. Gawlika. Water consumption related to different diets in Mediterranean cities. Science of the Total Environment 573, 96–105; 2016.
- [6] D. Vanham, B.M. Gawlik, G. Bidoglio. Food consumption and related water resources in Nordic cities. Ecological Indicators 74, 119–129; 2017
- [7] IWA, International Water Association. Alternative Water Resources: A Review of concepts, Solution and Experiences. Alternative Water Resources Cluster; 2015.
- [8] Ding Maa, Nan Lia, Wen-ying Chena. Analysis of the impacts of water constraints on China's power sector. Energy Procedia 75, 2665 – 2670; 2015.

-
- [9] Kim Choon Ng, Kyaw Thu, Youngdeuk Kim, Anutosh Chakraborty, Gary Amy. Adsorption desalination: An emerging low-cost thermal desalination method. *Desalination* 308, 161–179; 2013.
- [10] Sydney Miller, Hilla Shemer, Raphael Semiat. Energy and environmental issues in desalination. *Desalination* 366, 2–8; 2015.
- [11] Hilla Shemer, Raphael Semiat. Sustainable RO desalination – Energy demand and environmental impact. *Desalination* 424, 10–16; 2017.
- [12] V. Pankratz, F. Gasson T.J., IDA Desalination Yearbook 2015–2016, Oxford, UK, Global Water Intell; 2016.
- [13] Hongfei Zheng, General problems in seawater desalination, in "Solar Energy Desalination Technology", Chap. 1, pages 1-46; 2017.
- [14] Energy consumption and water production cost of conventional and renewable-energy-powered desalination processes. *Renewable and Sustainable Energy Reviews* 24, 343–356; 2013.
- [15] Prakash Narayan Govindan for Lienhard Research Group (Massachusetts Institute of Technology), Status of Humidification Dehumidification Desalination presented at *IDA World Congress on Desalination and Water Reuse*, Perth, September 4-9; 2011.
- [16] Joachim Koschikowski, Marcel Wiegand, Matthias Rommel. Solar thermal-driven desalination plants based on membrane distillation. *Desalination* 156, 295-304; 2003.
- [17] Sabine Lattemann, Thomas Höpner. Environmental impact and impact assessment of seawater desalination. *Desalination* 220, 1–15; 2008.
- [18] Thomas M. Missimera, Robert G. Malivab. Environmental issues in seawater reverse osmosis desalination: Intakes and outfalls. *Desalination* 434, 198–215; 2018.

-
- [19] David A. Roberts, Emma L. Johnston, Nathan A. Knott. Impacts of desalination plant discharges on the marine environment: A critical review of published studies. *Water research* 44, 5117-5128; 2010.
- [20] Roland V. Wahlgren. Atmospheric water vapour processor designs for potable water production: a review. *Water research*, 35(1),1-22; 2001.
- [21] Magrini A., Cattani L., Cartesegna M., Magnani L.. Production of water from the air: the environmental sustainability of air-conditioning systems through a more intelligent use of resources. The advantages of an integrated system. *Energy Procedia* 78, 1153 – 1158;2015.
- [22] V. Gentile, M. Simonetti, P. Finocchiaro, G.V. Fracastoro. Water production from the atmosphere in arid climates using low grade solar heat. In: *Proceedings of ISES Solar World Congress, Abu Dhabi,29oct.-2nov., 2017*.
- [23] P. Finocchiaro, M. Beccali, V. Gentile. Experimental results on adsorption beds for air dehumidification. *Internal journal of Refrigeration* 63, 100-112; 2016.
- [24] M. Dupont, B. Celestine, P.H. Nguyen, J. Merigoux, B. Brandon. Desiccant solar air conditioning in tropical climates-dynamic experimental and numerical studies of silica gel and activated alumina. *Solar Energy* 52, 509-518; 1994.
- [25] Y. Aristov. Challenging offers of material science for adsorption heat transformation:a review. *Applied thermal engineering* 50 (2), 1610-1618; 2013.
- [26] E. Ng, S. Mintova. Nanoporous materials with enhanced hydrophilicity and high water sorption capacity. *Microporous and Mesoporous Materials* 114, 2-26; 2008.
- [27] Melkon Tatliera, Gunther Munza, Stefan K. Henningera. Relation of water adsorption capacities of zeolites with their structural properties. *Microporous and Mesoporous Materials* 264, 70-75; 2018.

- [28] J.A. Martens, P. Jacobs. Crystalline microporous phosphates: a family of versatile catalysts and adsorbents. In: *Advanced Zeolite Science and Application, Studies in Surface Science and Catalysis (85)*, 653-685; 1994.
- [29] S. Henninger, F. Schmidt, H.-M. Henning. Water adsorption characteristics of novel materials for heat transformation applications. *Applied Thermal Engineering (30)*, 1692–1702.; 2010.
- [30] Marco Simonetti, Vincenzo Gentile, Gian Vincenzo Fracastoro, Angelo Freni, Luigi Calabrese, Giacomo Chiesa. Experimental testing of the buoyant functioning of a coil coated with SAPO34 zeolite, designed for solar DEC (Desiccant Evaporative Cooling) systems of buildings with natural ventilation. *Applied Thermal Engineering (103)*, 781–789; 2016.
- [31] A. Mahesh. Solar collectors and adsorption materials aspects of cooling system. *Renewable and Sustainable Energy Reviews (73)*, 1300–1312; 2017.
- [32] Yu.I. Aristov, M.M. Tokarev, G. Cacciola, G. Restuccia. Selective water sorbents for multiple applications: 1. CaCl₂ confined in mesopores of the silica gel: sorption properties. *React. Kinet. Cat. Lett. 59*, 325-334; 1996.
- [33] Yuri I. Aristov, Mikhail M. Tokarev, Angelo Freni, Ivan S. Glaznev, Giovanni Restuccia. Kinetics of water adsorption on silica Fuji Davison RD. *Microporous and Mesoporous Materials (96)*, 65–71; 2006.
- [34] Versteeg, H. K., & Malalasekera, W. *An Introduction to Computational Fluid Dynamics - The Finite Volume Method. (1 ed.)*. England, Longman Scientific & Technical. 1995.
- [35] Matthias Thommes, Katsumi Kaneko, Alexander V. Neimark, James P. Olivier, Francisco Rodriguez-Reinoso, Jean Rouquerol and Kenneth S.W. Sing. Physisorption of gases, with special reference to the evaluation of surface area and pore size distribution (IUPAC Technical Report). *Pure Appl. Chem.* 2015.
- [36] <http://www.ahmetcecen.tech/MultiPolyRegress-MatlabCentral/>

- [37] Michael B. Jakubinek, Bi-Zeng Zhan, Mary Anne White. Temperature-dependent thermal conductivity of powdered zeolite NaX. *Microporous and Mesoporous Materials* 103, 108–112; 2007.
- [38] Melkon Tatlier. Performances of MOF vs. zeolite coatings in adsorption cooling applications. *Applied Thermal Engineering* 113, 290–297; 2017.
- [39] <https://documentation.thesteveportal.plm.automation.siemens.com>